Journal of Physics B: Atomic,
Molecular and Optical Physics

PAPER

Theoretical investigations of $e^{\pm}$–CO scattering

To cite this article: M Masum Billah *et al* 2021 *J. Phys. B: At. Mol. Opt. Phys.* **54** 095203

IOP Publishing Journal of Physics B: Atomic, Molecular and Optical Physics

J. Phys. B: At. Mol. Opt. Phys. **54** (2021) 095203 (23pp) https://doi.org/10.1088/1361-6455/abf6b4

Theoretical investigations of $e^{\pm}$–CO scattering

M Masum Billah[1], Mahmudul H Khandker[1], M Shorifuddoza[2], M A Sayed[3], Hiroshi Watabe[4], A K F Haque[1,5,6,*] and M Alfaz Uddin[2]

[1] Atomic and Molecular Physics Lab, Department of Physics, University of Rajshahi, Rajshahi-6205, Bangladesh
[2] Department of Physics, Pabna University of Science and Technology, Pabna-6600, Bangladesh
[3] Department of Physics, Begum Rokeya University, Rangpur-5400, Bangladesh
[4] Division of Radiation Protection and Safety Control, Cyclotron and Radioisotope Center, Tohoku University, 6-3 Aoba, Aramaki, Aoba, Sendai 980-8578 Japan
[5] Nanosciences African network (NANOAFNET), Materials Research Group (MRG), iThemba LABS-National Research Foundation (NRF), 1 Old Faure Road, 7129, PO Box 722, Somerset West, Western Cape Province, South Africa
[6] UNESCO-UNISA Africa Chair in Nanosciences/Nanotechnology Laboratories, College of Graduate Studies, University of South Africa (UNISA), Muckleneuk Ridge, PO Box 392, Pretoria, South Africa

E-mail: fhaque@ru.ac.bd

Received 1 December 2020, revised 1 March 2021
Accepted for publication 9 April 2021
Published 13 May 2021

Abstract

The differential, integrated elastic, total, momentum transfer, viscosity cross sections and spin-polarization for electron and positron elastic scattering from carbon monoxide (CO) molecule are calculated for the energy range of 1 eV–10 keV. The work also includes the calculations of inelastic and total ionization cross sections for the same scattering system. Calculations of the above scattering observables for CO over such a wide range of energy are reported for the first time. Single scattering independent atom model (IAM) and the screening correction within the same framework, are used for the present analysis. Dirac partial wave analysis is used to calculate the phase-shifts required for the generation of the scattering observables, using a complex optical model potential. Comparison of our calculated results with the available experimental observations and other theoretical calculations is presented. The screening corrected independent atom model is found to provide better description of the results than the IAM.

Keywords: electron and positron-molecule scattering, carbon monoxide molecule, Dirac partial wave analysis, optical model, screening correction, independent atom model

(Some figures may appear in colour only in the online journal)

1. Introduction

Reliable data of the electron–atom/molecule collisions are of great importance in understanding the phenomena of planetary environments, features of interstellar objects, radiation chemistry, radiobiology, gaseous plasma and electron induced reactions on surfaces [1]. Electron scattering by molecules plays also an important role in modeling of cometary and interstellar plasmas [2]. Data of positron interactions with atoms and molecules have also great importance in astrophysics and biomedical applications requiring the above molecular scattering data as the inputs of several modeling software designed for the estimation of radiation induced damage to biological system [3]. Thus, for the enhancement of our knowledge about science of planetary, stellar and interstellar spaces and development of technologies, data on scattering of electron and positron from molecules is of indispensable [1].

* Author to whom any correspondence should be addressed.

CO is a simple diatomic, linear, weakly polar, heteronuclear molecule. It is important in comprehending and modeling of the atmospheric convection on Jupiter [4]. This molecule is one of the significant atmospheric constituents of venus, mars and also of comets. Besides these, CO is the 2nd most plentiful molecule in the interstellar space [5]. So, the study of electron and positron collisions with this molecule unravel useful information about the above systems.

Due to the complicated procedures for measurements, the experimental data of projectile–molecule scattering, related to various observables, very often than not, contain errors in normalization, magnitude and shape [1]. A theoretical model is essential to overcome the ambiguities in experimental measurements. If a theory is found consistent with several scattering observables of $e^{\pm}$–molecule scattering, it can be used for the predictive purposes, where an experiment is difficult to perform, and correction of errors, if any, of measured data.

To explain the spin polarization during scattering of electron and positron, it is necessary to include spin–orbit interaction term in Schrödinger equation. But, in Dirac's relativistic equation, this term is intrinsically incorporated [6]. This is why, we adopt Dirac partial wave analysis with complex optical model potential (OMP), to calculate differential cross section (DCS), integrated elastic cross section (IECS), momentum transfer cross section (MTCS), viscosity cross section (VCS), inelastic cross section (INCS), total cross section (TCS), total ionization cross section (TICS) and spin polarization for the scattering of electron and positron from carbon monoxide (CO) molecule.

The projectile–molecule interaction is not spherically symmetric, so the partial wave method cannot be applied directly for the generation of observable quantities for the projectile molecule scattering. Various approximate methods are used to calculate these observables for modeling of different phenomena concerning the scattering. In the additive model, the cross sections for elastic scattering are derived as the sum of the cross sections of the individual atoms composing a molecule. This method ignores the chemical-bonding and aggregation effects of a molecule. The charge distribution of bound electrons of an atom in molecule is different from that of the free state of that atom due to the overlapping of atomic orbitals in the formation of a molecule. In the IAM approach, the scattering of electron or positron is described assuming the free-atom potential for the interaction of a projectile with an atom of a molecule. To obtain the differential and other cross sections, the scattered wave from a molecule is approximated as the coherent sum of those from the individual atoms of the molecule. In these approaches, the projectile–molecule interaction is reduced to the projectile–atom interaction in the collision dynamics designed for the calculation of projectile–atom scattering.

In OMP, the non-local potential, is approximated by a local complex potential and the many-body problem is reduced to one-body problem. This procedure exemplifies the algorithm of generating the cross sections from the solution of Dirac's equation. The complex $e^{\pm}$–atom OMP has both real and imaginary parts. The real part comprises three components: static, correlation-polarization and exchange potentials. The static potential originates from the interaction between the projectile (e^-/e^+) and bound electrons and nuclear protons of the atom. So, this potential is same both for electron and positron except the sign. The correlation-polarization potential results from the distortion of atomic charge distribution under the influence of incident particle's electric field. This component of OMP is a combination of a long-range and a short-range part. The exchange potential is the result of exchange between projectile electrons and the bound electrons of target atom. It is a short-range interaction. Above the inelastic threshold energy, there is a loss of incident flux during the collision course. This loss of flux is represented by the imaginary part of the potential.

In our previous study [6], we have used additivity rule (AR) to describe $e^{\pm}$–N_2 scattering. Although this method ignores chemical-binding and aggregation effects, it successfully produced the scattering observables in case of simple di-atomic homo nuclear nitrogen molecule. The charge distribution of electrons in an isolated atom varies from that of a bound atom in a molecule of the same element. This variation has only small influence on the elastic DCS, for projectiles with energies higher than a few 100 eV. The aggregation effect (having multiple atoms bound together in a well-defined relative positions), has more strong influence on the DCS [7]. For these limitations of AR approximation, this work uses IAM. According to this model, the target molecule is approximately replaced by their constituent atoms in the corresponding positions. The main drawback of this model is not to consider multiple scattering of the projectile from the constituent atoms of the molecule, making it applicable only at comparatively high energies (>100 eV) [8]. Another reason of low energy failure of IAM is ignoring the mutual overlapping of nearby atomic cross sections. To overcome this problem, Blanco and Garcia [9] proposed a simple screening correction for overlapping of nearby atoms in molecules. Later, Blanco *et al* [8] applied the same procedure (screening correction), in the fold of non-relativistic Schrödinger theory to the independent atom model (IAM), resulting in a significant improvement of the quality of various cross sections in the low energy domain. Gholami *et al* [10] applied this screening correction in the Dirac relativistic partial wave analysis to report electron impact TCS, IECS, INCS and DCS on molecules. We apply this model to the test case of $e^{\pm}$–CO scattering to examine the results. We observe substantial improvement for all the scattering observables in low to intermediate energy regions. The comparison of our results, with experimental observations as well as other theoretical calculations available in the literature, is encouraging.

The scattering of electron and positron off CO has been studied extensively by both theoretical and experimental methods. Tanaka *et al* [4] measured DCS, IECS and MTCS over the energy range 3–100 eV. Gibson *et al* [11] published the measurements on DCS (1–30 eV). Gote and Ehrhardt [12] reported DCS (10–200 eV) for electron scattering between 10° and 160°. Middleton *et al* [13] measured DCS over the energy range 20–50 eV. Maji *et al* [14] reported DCS of 300–1300 eV, and theoretical calculations with 3 different approaches. Przybyla *et al* [15] have given experimental data of DCSs for quasielastic scattering of positrons by CO for the

energy range 5.25–100 eV. All of these experiments were done by crossed-beam method. Nickel *et al* [16] measured DCS (20–100 eV) using a relative flow technique. DuBois and Rudd [17] reported DCS of 200–800 eV energy for scattering of electron by static CO gas target. Bromberg [18] measured DCS data for the energy range 300–500 eV. Experimental TCS data for electron scattering have been published by Szmytkowski *et al* [1], Garcia *et al* [19], Karwasz *et al* [20] and Xing *et al* [21]. Measurements of TCS for both electron and positron are reported by Kwan *et al* [22], Sueoko and Mori [23]. Furthermore, Zecca *et al* [24] and Sueoka and Hamada [25] reported measured TCS for positron scattering. Electron impact experimental TICS are reported by Rapp and Golden [26], Asundi *et al* [27], Orient and Srivastava [28], Tian and Vidal [29]. Alan [30] reported measurements of IECS and MTCS for the energy range 0.5–10 eV. Marler and Surko [31] and Bluhme *et al* [32] reported experimental data on TICS for positron scattering.

Literature shows theoretical studies on $e^{\pm}$ scattering from CO molecule. Jain [33] reported elastic DCS, MTCS and IECS using two potential approach in the energy range 40–800 eV. A sum of short- and long-range potentials is used as the total interaction potential. Jain *et al* [2] reported elastic DCS over 50–200 eV, IECS and MTCS for the energy range 50–800 eV. The intramolecular multiple scattering effect is embedded in two-potential coherent approach in their calculations. Lee *et al* [34] used a complex optical potential derived from a fully molecular wavefunction within the framework of the Schwinger variational iterative method combined with the distorted-wave approximation to calculate DCS, IECS, MTCS and TCS for e^-–CO scattering in the energy range 2–500 eV. Castro *et al* [35] reported DCS in the energy range 20–300 eV, INCS and TCS for electron scattering in 15–1000 eV energy range. In their study they used the third version of quasi-free scattering model with modified absorption potential. Using modified additivity approach, Joshipura and Patel [36] calculated TCS and INCS for electron scattering in the energy range 10–2000 eV. Itikawa [5] and Kanik *et al* [37] reported recommended cross sections for electron scattering. Vinodkumar *et al* [38] reported TICS from threshold to 5000 eV using complex spherical potential-ionization contribution method for electron scattering. Hwang *et al* [39] reported electron impact TICS using binary-encounter Bethe model from threshold to 1000 eV energy range. Jain and Baluja [40] reported TCS, IECS and INCS using the approach based on spherical complex optical potential (SCOP) of the electron–molecule system. Land [41] reported theoretical MTCS using the spherical harmonic expansion approximation. Kothari and Joshipura [42] reported TCS, TICS, IECS and INCS of positron impact over the energy range 15–2000 eV, using complex spherical potential formalism. Baluja and Jain [43] calculated TCS of positron scattering in the energy range 10–5000 eV. Singh *et al* [3] published calculations TCS and INCS over the energy range from near positronium (Ps) formation threshold to 5000 eV with a modified version of SCOP formalism. Reid and Wadehra [44] presented TCS and IECS in the energy range from 100 to 5000 eV using parameter-free interaction potentials along with the AR. Arretche *et al* [45] published their calculations on positron impact DCS and TCS using the method of continued fractions and iterative Schwinger variational methods. Dora and Tennyson [46] reported resonance energies and widths of long-lived metastable electronic states of the CO^- anion using *R*-matrix method. Using the same method, Dora *et al* [47] calculated higher lying resonances in low energy electron scattering. Sun *et al* [48] published integral and differential excitation cross sections of the valence states using the Schwinger multichannel variational method. Zawadzki *et al* [49] reported DCS for electron excitation of the three lowest excited states experimentally using low-energy electron energy-loss spectroscopy and theoretically using the *R*-matrix method. Silva *et al* [50] investigated positron impact theoretical cross sections for electronic excitation by using Schwinger multichannel method.

The organization of this article is as follows. In section 2, the outline of the theory is presented. Section 3 provides the discussion of our results in comparison with those from other calculations and measurements. In section 4, conclusion is drawn on our findings.

2. Theory

2.1. The interaction potential

The complex OMP of the projectile–atom interaction, as in [7] is given by following form

$$\begin{aligned} V(r) &= V_{\text{real}}(r) - iW_{\text{abs}}(r) \\ &= V_{\text{st}}(r) + V_{\text{ex}}(r) + V_{\text{cp}}(r) - iW_{\text{abs}}(r). \end{aligned} \tag{1}$$

Here, $V_{\text{st}}(r)$, $V_{\text{ex}}(r)$ and $V_{\text{cp}}(r)$, represent the static, exchange and correlation-polarization potentials respectively and the imaginary part, $W_{\text{abs}}(r)$, the magnitude of the absorption potential. For positron, exchange part is zero. The details of the procedure of generation, expressions of these potential components and the collision dynamics are provided in reference [6] and the references therein.

Static potential is the electrostatic interaction of the projectile (electron or positron) with atomic charge distribution (nuclear proton and electron cloud). The proton and electron number density functions $\varrho(r)$ are normalized according to the following relation

$$\int \varrho(r) 4\pi r^2 dr = Z. \tag{2}$$

Here, Z is the atomic number of the atom. To model the nuclear potential, Fermi nuclear density function of the following form [51] are used for the constituent atoms

$$\varrho_n = \frac{\varrho_0}{1 + e^{(r-R_n)/a}}. \tag{3}$$

Here $a = 0.546$ fm, is the diffuseness parameter and the half-way radius $R_n = 1.944$ fm and 2.140 fm respectively for ^{6}C and ^{8}O nuclei. ϱ_0 is normalization constant. Dirac–Fock electron density generated within the framework of multi-configuration technique by Desclaux code [52] is used to generate the components of the optical potential.

The exchange interaction, a unique feature of electron–atom interaction, arises from the anti-symmetrization

of the wave function of the whole system comprising the atomic and incident electrons. It leads to a set of coupled integro-differential equations and gives rise to a nonlocal interaction. The semi-classical local exchange potential of Furness and McCarthy [6, 53] derived from the non-local exchange interaction using the WKB like wave functions is used in the present study.

The global correlation-polarization potential is obtained by the combination of the long-range Buckingham potential $V_{\rm p}(r)$ and the short-range LDA correlation potential $V_{\rm co}^{(r)}$ as follows [54],

$$V_{\rm cp}^{\pm}(r) \equiv \begin{cases} \max\left\{V_{\rm co}^{\pm}(r), V_{\rm p}(r)\right\} & \text{if} \quad r < r_{\rm cp} \\ V_{\rm p}(r) & \text{if } r \geqslant r_{\rm cp}. \end{cases} \tag{4}$$

where $r_{\rm cp}$ is the outer radius at which $V_{\rm co}^{(r)}$ and $V_{\rm p}(r)$ cross first. $V_{\rm co}^{(r)}$ for electron and positron are taken from Perdew and Zunger [55] and Jain [56] respectively as in reference [6].

Projectiles with impact energy greater than the inelastic threshold are absorbed due to the opening of inelastic channels. A negative imaginary potential $-{\rm i}W_{\rm abs}(r)$, is included in the OMP to describe this effect. In present work, we adopt, for $W_{\rm abs}(r)$, the potential proposed by Salvat [7, 54], which is given by

$$W_{\rm abs} = \sqrt{\frac{2(E_{\rm L}+m_{\rm e}c^2)^2}{m_{\rm e}c^2(E_{\rm L}+2m_{\rm e}c^2)}} \times A_{\rm abs}\frac{\hbar}{2}\left[v_{\rm L}^{nr}\varrho_{\rm e}(r)\sigma_{\rm bc}(E_{\rm L},\varrho_{\rm e},\Delta)\right]. \tag{5}$$

Here $A_{\rm abs}$ is a projectile-target dependent parameter. In present study, its value is 2 for both electron and positron.

2.2. Partial wave analysis

The scattering of electrons and positrons by a central field $V(r)$ is completely described by the direct and spin flip scattering amplitudes, given by [57, 58]

$$f(\theta) = \frac{1}{2ik}\sum_{l=0}^{\infty}\{(\ell+1)\left[\exp(2i\delta_{\kappa=-\ell-1})-1\right] + \ell\left[\exp(2i\delta_{\kappa=\ell})-1\right]\}P_{\ell}(\cos\,\theta), \tag{6}$$

and

$$g(\theta) = \frac{1}{2ik}\sum_{l=0}^{\infty}\left[\exp(2i\delta_{\kappa=\ell})-\exp(2i\delta_{\kappa=-\ell-1})\right]\times P_{\ell}^{1}(\cos\,\theta) \tag{7}$$

respectively. Here, k is the relativistic wave number of the projectile which is related to the kinetic energy E_i by

$$(c\hbar k)^2 = E_i(E_i+2m_{\rm e}c^2). \tag{8}$$

$P_{\ell}(\cos\theta)$ and $P_{\ell}^{1}(\cos\,\theta)$ are the Legendre polynomials and associated Legendre functions respectively. κ is relativistic quantum number defined as $\kappa=(\ell-j)(2j+1)$, where j and ℓ are the total and orbital angular momentum quantum numbers that are both determined by the value of κ as $j=|\kappa|-1/2$, $\ell=j+\kappa/(2|\kappa|)$.

The partial wave series converge very slowly for the small angle elastic scattering by molecules. There is scope for 25 000 partial waves [7, 59]. Angular momentum is increased up to a certain maximum for which the absolute value of the phase-shift is less than 10^{-9}. At this point partial wave expression for $f(\theta)$ and $g(\theta)$ converge to the required accuracy (usually more than six decimal places) for all angles.

The partial-wave method is not applicable directly on the $e^{\pm}$–molecule interaction because the interaction potential in these cases is not spherically symmetric. In the IAM, the direct and spin flip scattering amplitudes to describe the scattering from a molecule with a given orientation are given by [58]

$$F(\theta) = \sum_i \exp(i\mathbf{q}.\mathbf{r}_i)f_i(\theta)$$

and

$$G(\theta) = \sum_i \exp(i\mathbf{q}.\mathbf{r}_i)g_i(\theta) \tag{9}$$

here $\hbar\mathbf{q}$ is the momentum transfer, $\mathbf{r}_i$ is the position vector for the nucleus of the ith atom, relative to an arbitrary origin and $f_i(\theta)$ and $g_i(\theta)$ are the scattering amplitudes for the constituent free atom of element. The corresponding DCS, obtained by averaging the orientations of all the randomly oriented molecules, is given by

$$\frac{d\sigma}{d\Omega} = \langle|F(\theta)|^2+|G(\theta)|^2\rangle \tag{10}$$

$$= \sum_{i,j}\frac{\sin(qr_{ij})}{qr_{ij}}[f_i(\theta)f_j^*(\theta)+g_i(\theta)g_j^*(\theta)] \tag{11}$$

$$= \sum_i[|f_i(\theta)|^2+|g_i(\theta)|^2] + \sum_{i\neq j}\frac{\sin(qr_{ij})}{qr_{ij}}[f_i(\theta)f_j^*(\theta)+g_i(\theta)g_j^*(\theta)] \tag{12}$$

where $q=2k\sin(\theta/2)$, r_{ij} is the distance between ith and jth atoms, $\sin(qr_{ij})/qr_{ij}=1$ when $qr_{ij}=0$ and the term $\sum_{i\neq j}$ represents interference contribution to the molecular DCS.

The integrated elastic $\sigma_{\rm el}$, the momentum transfer $\sigma_{\rm m}$ and the viscosity σ_v cross sections for the projectile–molecule scattering are expressed in terms of the DCS as

$$\sigma_{\rm el} = \int\frac{d\sigma}{d\Omega}d\Omega = 2\pi\int_0^{\pi}\left(\frac{d\sigma}{d\Omega}\right)\sin(\theta)d\theta \tag{13}$$

$$\sigma_{\rm m} = 2\pi\int_0^{\pi}(1-\cos\,\theta)\left(\frac{d\sigma}{d\Omega}\right)\sin(\theta)d\theta \tag{14}$$

$$\sigma_{\rm v} = 3\pi\int_0^{\pi}\left[1-(\cos\,\theta)^2\right]\left(\frac{d\sigma}{d\Omega}\right)\sin(\theta)d\theta. \tag{15}$$

The molecular total cross section (TCS) $\sigma_{\rm tot}$ for both electron and positron scattering, sum of integrated elastic ($\sigma_{\rm el}$) and absorption cross section ($\sigma_{\rm inel}$), can be obtained from the

following expression

$$\sigma_{\rm tot} = \sigma_{\rm el} + \sigma_{\rm inel} = \frac{4\pi}{k}\sum_i {\rm Im} f_i(0), \tag{16}$$

where ${\rm Im}f_i(0)$ denotes the imaginary part of direct scattering amplitude in the forward direction at $\theta = 0^\circ$ for the ith atom.

To account for the mutual overlapping of nearby atoms in molecule, Blanco and Garcia [9] proposed a correction which is known as the screening correction. According to this formulation [9], the screening correcting factors s_i, $(0 \leqslant s_i \leqslant 1)$ for ith and jth atoms of a molecule are given by,

$$s_i = 1 - \frac{\varepsilon_i^{(2)}}{2!} + \frac{\varepsilon_i^{(3)}}{3!} - \frac{\varepsilon_i^{(4)}}{4!} + \cdots\cdots \tag{17}$$

where

$$\varepsilon_i^{(m)} = \frac{N-m+1}{N-1}\sum_{i\neq j}\frac{\sigma_j \varepsilon_j^{(m-1)}}{\alpha_{ij}} \quad ({\rm m} = 2, \ldots\ldots, N), \tag{18}$$

represents m-atom overlapping. N, is the number of atoms in the target molecule. $\alpha_{ij} = \max(4\pi r_{ij}^2, \sigma_i, \sigma_j)$, σ_i and σ_j are the atomic TCSs for the ith and jth atoms of the molecule. Since CO is a diatomic molecule, $N = 2$ and the equation (17) takes the following form

$$s_i = 1 - \frac{1}{2}\sum_{i\neq j}\frac{\sigma_j}{\alpha_{ij}}. \tag{19}$$

The coefficients s_i reduce the contribution of constituent atoms to the molecular cross section. From the formulation of [8], another factor ν_{ij} is used to the positive values of $\sum_{i\neq j}\nu_{ij}s_i s_j \frac{\sin(qr_{ij})}{qr_{ij}}[f_i(\theta)f_j^*(\theta)]$, which is defined as $\nu_{ij} = r_{ij}^2/(r_{ij}^2 + \rho_{ij}^2)$, with length dimensional parameter $\rho_{ij} = \max(\sqrt{\sigma_i/\pi}, \sqrt{\sigma_j/\pi}, 1/k)$. Here $(\sqrt{\sigma/\pi})$ represents the radius of a circle of area σ. So, the expression for the differential scattering cross section with the correcting factors (s_i, ν_{ij}) i.e. the screening corrected version of equation (12)

$$\left(\frac{d\sigma}{d\Omega}\right)^{\rm s} = \sum_i s_i^2[|f_i(\theta)|^2 + |g_i(\theta)|^2] + \sum_{i\neq j}\nu_{ij}s_i s_j \frac{\sin(qr_{ij})}{qr_{ij}}[f_i(\theta)f_j^*(\theta) + g_i(\theta)g_j^*(\theta)] \tag{20}$$

.The first summation in equation (20) accounts for each atomic contribution, reduced by s_i factors and the second one for the reduced interference contributions. The screening corrected integrated elastic $\sigma_{\rm el}^{\rm s}$, momentum transfer $\sigma_{\rm m}^{\rm s}$ and viscosity $\sigma_{\rm v}^{\rm s}$ cross sections are obtained from equations (13)–(15) replacing $(\frac{d\sigma}{d\Omega})$ with $(\frac{d\sigma}{d\Omega})^{\rm s}$ from equation (20).

The screening corrected total cross section $\sigma_{\rm tot}^{\rm s}$ is given by

$$\sigma_{\rm tot}^{\rm s} = \sigma_{\rm el}^{\rm s} + \sigma_{\rm inel}^{\rm s} = \sum_i s_i(\sigma_{\rm el} + \sigma_{\rm inel}) = \sum_i s_i \sigma_{\rm tot}. \tag{21}$$

The asymmetry function of randomly oriented molecule is

$$S(\theta) = i\frac{\langle F(\theta)G^*(\theta) - F^*(\theta)G(\theta)\rangle}{\langle |F(\theta)|^2 + |G(\theta)|^2\rangle}. \tag{22}$$

Since CO is a polar molecule, the interaction energy of the projectile with the permanent dipole moment vanishes when it is averaged over different molecular orientations and can be neglected in elastic scattering calculations, as a first approximation. For the correct large-r behavior of the polarization field, it is assumed that the effective dipole polarizability $\alpha_{\rm d,eff}(i)$ of the ith atom of the molecule is proportional to the polarizability of the free atom, $\alpha_{\rm d}(i)$. The molecular polarizability must be equal to the sum of effective atomic polarizabilities. For the calculations of scattering amplitudes from the ith atom, we have used the effective polarizability

$$\alpha_{\rm d,eff}(i) = \alpha_{\rm d}^{\rm mol}\,\alpha_{\rm d}(i)\left[\sum_j \alpha_{\rm d}(j)\right]^{-1}, \tag{23}$$

here the summation extends over all the constituent atoms in molecule. The atomic polarizabilities for carbon and oxygen are used 1.76 $\mathring{A}^3$ [60] and 0.802 $\mathring{A}^3$ [60] respectively. The molecular polaziability of CO molecule is 1.95 $\mathring{A}^3$ [42]. In the IAM approximation the effective atomic polarizability defined by equation (23) is used to calculate the polarization potential $V_{\rm p}(r)$ for an atom. The 1st molecular excitation energy is used 6.3 eV [61] for present analysis.

Total INCS ($\sigma_{\rm inel}$) and ionization cross section ($\sigma_{\rm ion}$) satisfy the following relation

$$\sigma_{\rm inel} \geqslant \sigma_{\rm ion} \tag{24}$$

as the former itself is partitioned into excitation and ionization cross section. Ionization cross section ($\sigma_{\rm ion}$) can be calculated from the following ratio (energy dependent) as is done in [62, 63],

$$R(E_i) = \frac{\sigma_{\rm ion}(E_i)}{\sigma_{\rm inel}(E_i)}. \tag{25}$$

The ratio $R(E_i)$ is a continuous function of energy. For $E_i > I$ (ionization potential), this function is fitted to the equation

$$R(E_i) = 1 - C1\left[\frac{C2}{U+A} + \frac{\ln U}{U}\right], \tag{26}$$

where $U = E_i/I$ is the reduced energy. The adjustable parameters $C1$, $C2$ and A are determined using the following conditions.

$$R(E_i) = \begin{cases} 0 & \text{for} \quad E_i \leqslant I, \\ R_{\rm p} & \text{for} \quad E_i = E_{\rm p} \\ R_{\rm F} & \text{for} \quad E_i \geqslant E_{\rm F} > E_{\rm P}. \end{cases} \tag{27}$$

First condition of equation (27) implies that, no ionization takes place below the ionization threshold energy of the molecule. Here, $E_{\rm p}$ is the impact energy at which absorption gets its maximum and $R_{\rm p}$ represents R at $E_i = E_{\rm p}$. In present analysis, we observe $E_{\rm p} = 100$ eV for both projectiles. From the discussion of references [62–64], we choose $R_{\rm p} = 0.8$. At incident energies $E_i \geqslant E_{\rm F}$, beyond the peak position $E_{\rm p}$, the value of R increases to $R_{\rm F}$ (very close to 1). However, it is observed that maximum ionization ($R(E_i) = 1$) does not happen even at high energies suggests that $R(E_i)$ must be less than one. To get optimal fit with the experimental observations, the

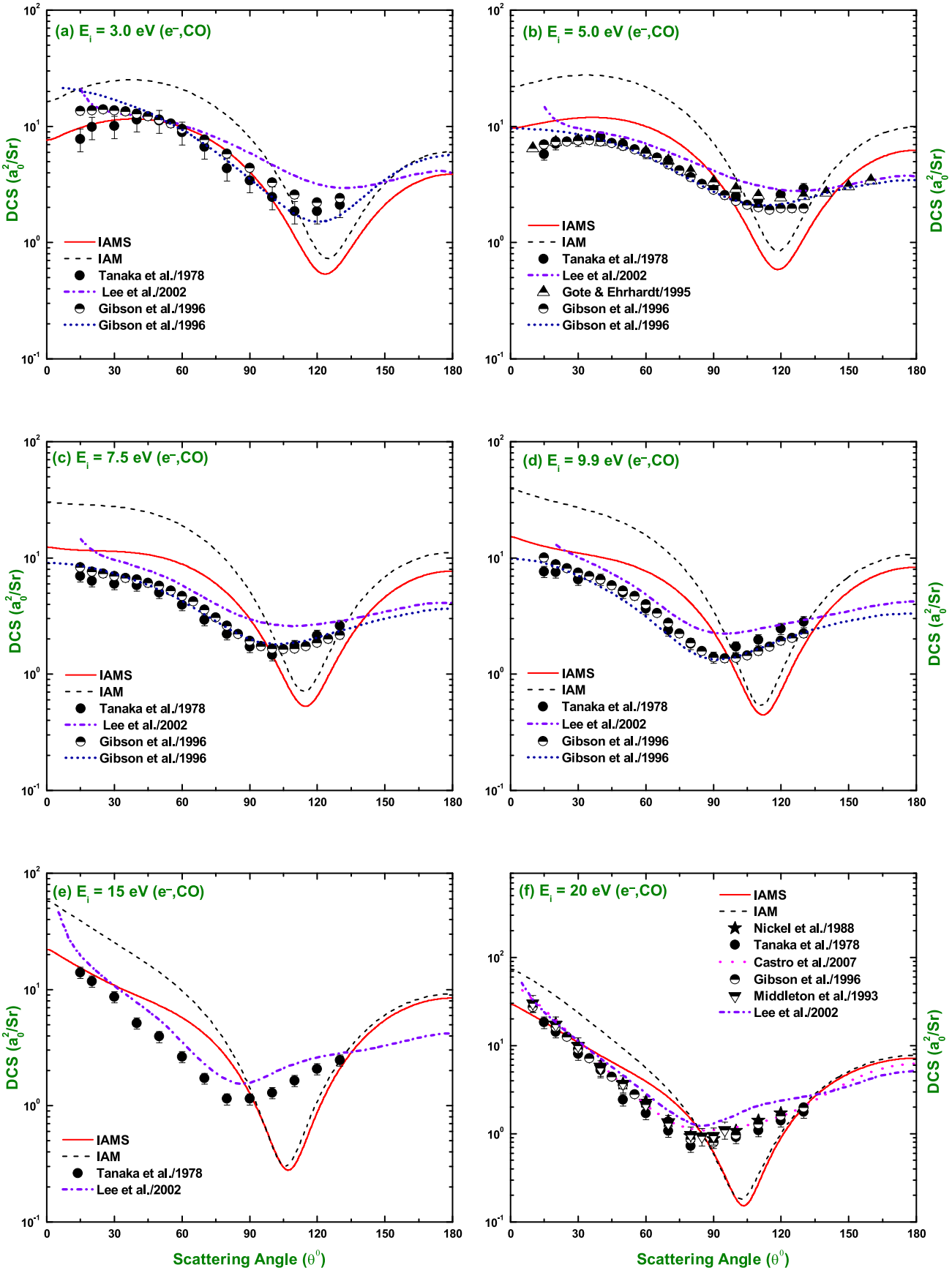

Figure 1. DCS (a_0^2/Sr) for the elastic scattering of electrons from CO at energies 3, 5, 7.5, 9.9, 15 and 20 eV. Theoretical: IAM—independent atom model, IAMS—independent atom model with screening correction, Gibson *et al* [11], Lee *et al* [34] and Castro *et al* [35]. Experimental: Tanaka *et al* [4], Gibson *et al* [11], Gote and Ehrhardt [12], Middleton *et al* [13] and Nickel *et al* [16].

value of R_F is chosen as 0.95 at $E_F = 500$ eV. The numerical values of the parameters $C1$, $C2$ and A are, respectively, found to be -1.263, -5.886, 6.436 both for electron and positron scattering. These values are obtained from the solutions of equation (27) using a FORTRAN program.

3. Results and discussions

In this work, the ELSEPA code [7] is used for the calculation of the scattering cross sections of electrons and positrons by CO molecule. DCSs for electron scattering calculated for a wide range of energy (3.0 eV–10 keV) are compared with the experimental measurements [4, 11–14, 16–18] and the theoretical calculations [14, 33–35]. DCSs for positron scattering are calculated for the energy range 5.25 eV–10 keV. TCSs, TICSs, IECSs, INCSs, MTCSs and VICSs for both the projectiles are calculated for the energy range 1 eV–10 keV.

In figures 1(a)–(f), we present our calculated DCS (IAM and IAMS) at energies 3, 5, 7.5, 9.9, 15 and 20 eV. At these energies both of our approaches show noticeable disagreement with the experiments [4, 11–13], but agree with the number of minima with shifts in positions. At 15 and 20 eV, both IAM and IAMS produce deep minimum at $\sim 100^\circ$ while the experimental minimum is observed at $\sim 80^\circ$. Calculations of Lee *et al* [34] show better agreement than our works, with the experimental data at these energies. The predictions of Lee *et al* [34] and Castro *et al* [35] for DCS at 20 eV, reasonably agree with the experimental observations. *R*-matrix calculation of Gibson *et al* [11] shows a good agreement in shape and magnitude except the forward angle ($<45^\circ$) at energies 3 and 5 eV. Our results produced by IAM and IAMS show disagreements with the experimental data at most of the angular points at these energies. This is due to the resonant scattering from the isolated states of the constituent atoms of CO and that the OMP does not take into consideration this indirect process of scattering.

In figures 2(a)–(f), we present our DCS calculations for electron scattering at 25, 30, 40, 50, 60 and 70 eV and compare with experimental data [4, 11–13, 16] and theoretical calculations [34, 35]. The most significant feature in the figure is the reduced values of DCS of IAMS than that of IAM, specially at low angle region, which are consistent with experimental observations. At 30 eV, the IAMS model shows reasonably good agreement with experiments [4, 11, 13] up to 80°. Theoretical calculations of [34] overestimate, whereas the present predictions underestimate the experimental data at minimum. At 40 eV, both of our models produce reasonably good agreement with slight underestimation at minimum. At energy 50 eV, our present IAMS and those of [35] show quite reasonable agreement with experimental data [4, 12, 13, 16] except at 130° and beyond. The calculation of [34] overestimates the experimental data in and around the minimum. We see an excellent agreement of IMAS with the experimental data at 60, 70, 80 and 90 eV, both in shape and magnitude. At these energies, IAM overestimates the experimental cross sections in forward angles. As expected, the inclusion of screening effect makes this theory effective to describe DCS of e^-–CO scattering from 50 eV. In the low energy (<50 eV) region, the inconsistent behavior of our calculations with data might be due to ignoring of the multiple scattering of electrons and positrons from the constituent atoms in the target molecule and structure effect.

In figures 3–5, we compare our results with the available measurements [4, 12, 14, 16–18] and theoretical calculations [14, 33–35]. At 75 eV, our IAMS agrees reasonably with the experimental data up to 100° beyond which it does not. At this energy, DCS values of [34] overestimate the experimental data except at lower angles. IAMS is far better than the calculation of [34]. At energies 80–150 eV, we see a reasonably good agreement of IAMS with existing theoretical and experimental data.

At 175 and 700 eV, both of our calculations (IAM and IAMS) are reasonably in concord with experimental data [12, 14]. At energies 200, 300, 400, 500 and 800 eV, we see close agreement of our calculated DCSs with the measurements of [17, 18] and an available calculations of [34]. At 200 eV, we observe significant difference in the experimental cross sections of Gote and Ehrhardt [12] and Dubois and Rudd [17] beyond 90°, DCS of [17] is 54% higher than that of [12] for the angle 110°. Deviation of our calculations from [12] at 125 and 150 eV energies (see the figures 3(e) and (f)) in the aforementioned angular range is not more than 54%. At 300 and 500 eV, the calculation of Maji *et al* [14] is not consistent with any set of experimental data. At 400 and 800 eV, our predictions and those of Jain [33] produce close agreements with experimental data of [17, 18]. For the energies at 700 and 900 eV, we see reasonably a good agreement of the calculations of Maji *et al* [14] and ours with their experimental data. The former calculations are only available within the data range. At 1100 eV, our calculations fairly agree with the experimental measurements and calculations of [14] with slight differences in magnitude. If the projectile energy increases, the interaction time will be shorter and consequently cross sections will be lower. At 1300 eV, both the experimental data and calculations of [14] are almost 10 times smaller than our calculations.

In figures 6(a)–(d), we present the calculated cross sections at energies 1500 to 10 000 eV. We do it for future reference and to see the trend of energy variation of DCS. One important point to notice that at higher energies both IAM and IAMS give almost the same results. This is because of the corresponding de Broglie wavelengths of the projectile at these energies are small enough compared to the inter-atomic distances of the target molecules. Incident particles are participating in the collision courses with all the atoms (inside the target molecule) independently without any kind of geometrical overlapping among them.

In figure 7, we have plotted the experimental data [4, 11–14, 16–18] with our screening corrected DCS over the energy range 1 eV–10 keV at angles 30°, 60°, 90° and 120°. We find our IAMS calculations closely agree, at all angles, with the whole experimental data range except at the backward angle 120° below about 20 eV. We also observe that the experimental cross sections show a much more larger spreading between different data sets at some energies, signifying that a theoretical method is very much essential to remove the discrepancies

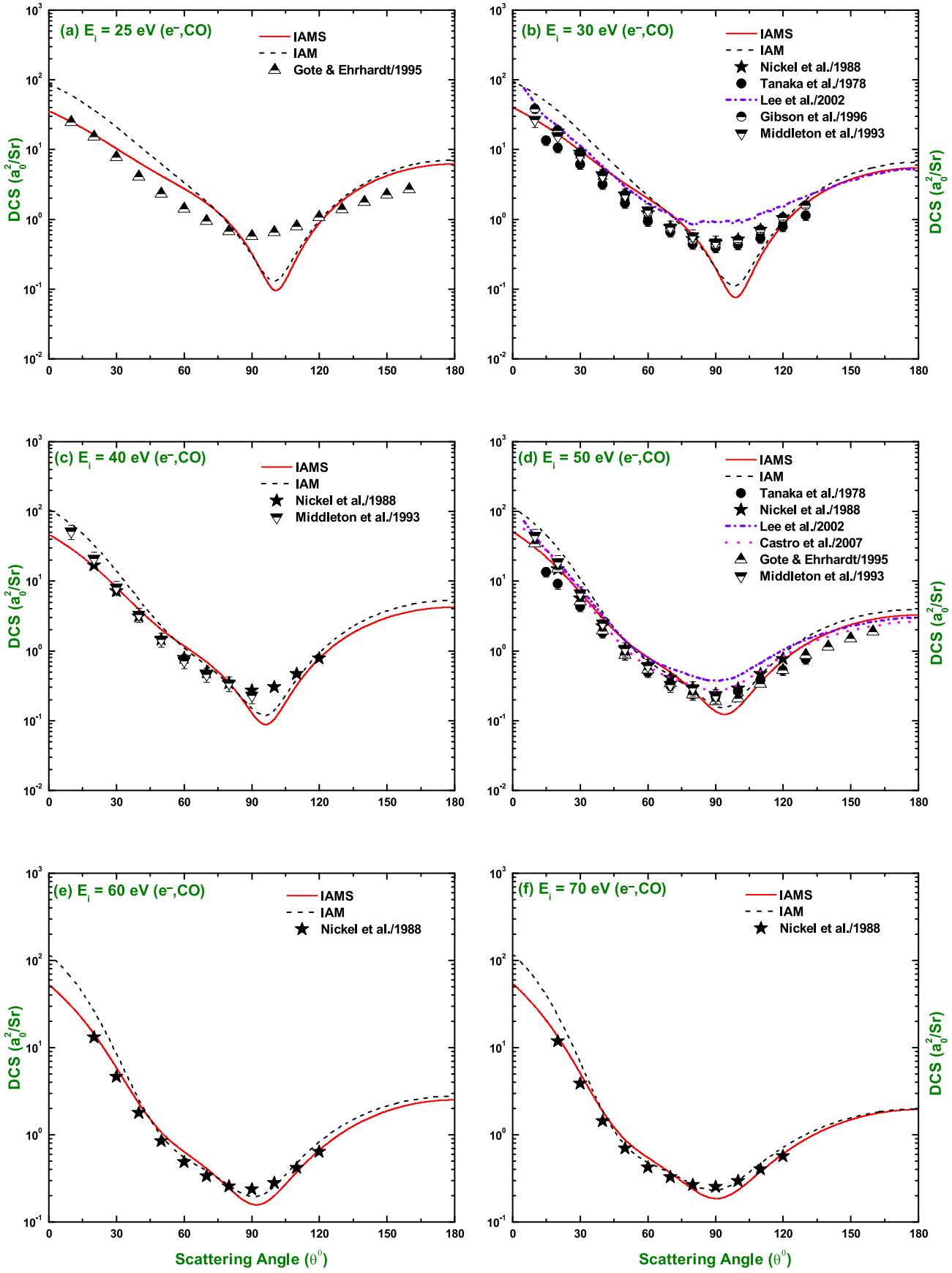

Figure 2. DCS (a_0^2/Sr) for the same as in figure 1 at energies 25, 30, 40, 50, 60 and 70 eV. Theoretical: references in figure 1. Experimental: references in figure 1.

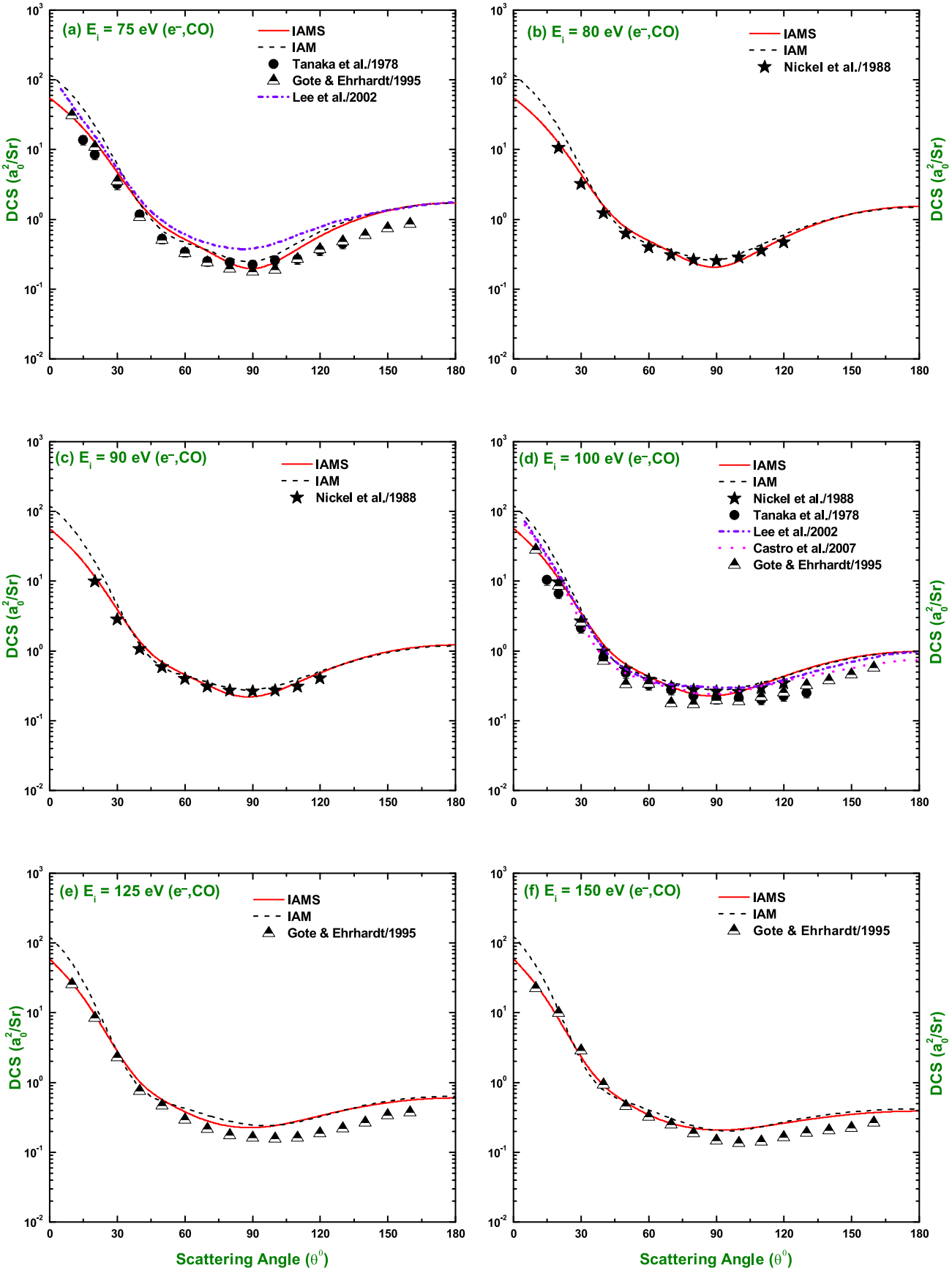

Figure 3. DCS (a_0^2/Sr) for the same as in figure 1 at energies 75, 80, 90, 100, 125 and 150 eV. Theoretical: references in figure 1. Experimental: references in figure 1.

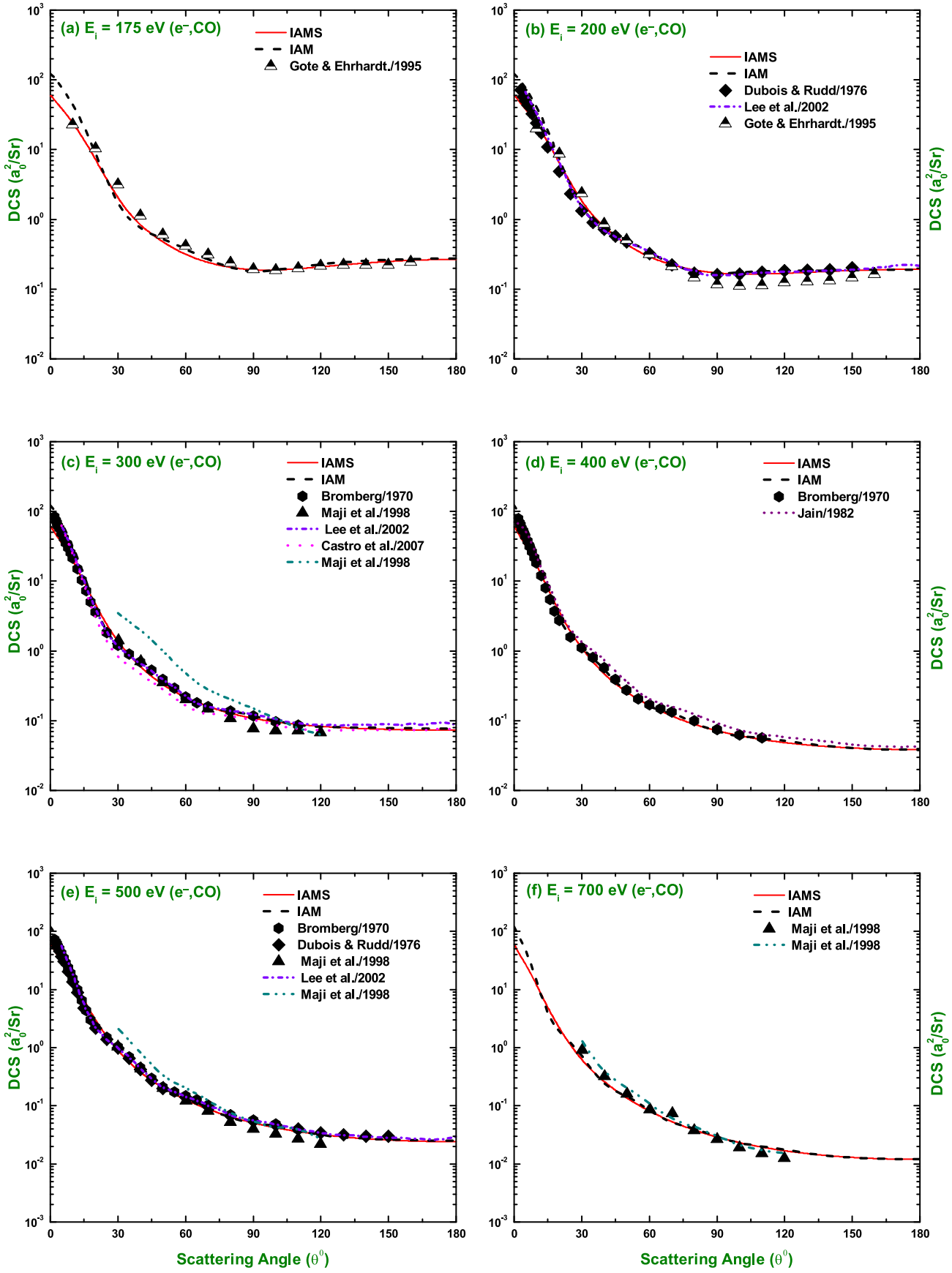

Figure 4. DCS (a_0^2/Sr) for the same as in figure 1 at energies 175, 200, 300, 400, 500 and 700 eV. Theoretical: references in figure 1, Maji *et al* [14] and Jain [33]. Experimental: references in figure 1, Maji *et al* [14], DuBois and Rudd [17] and Bromberg [18].

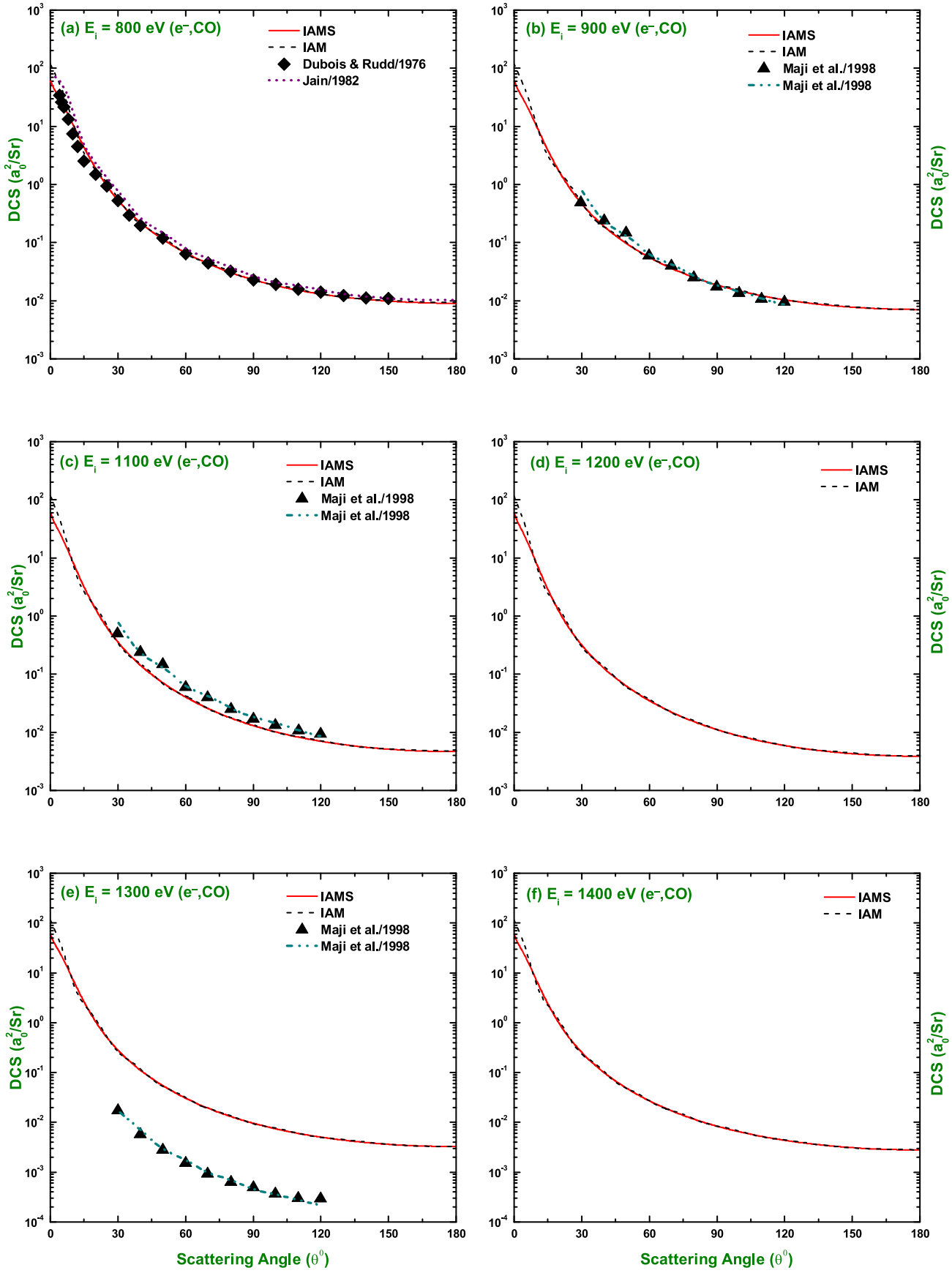

Figure 5. DCS (a_0^2/Sr) for the same as in figure 1 at energies 800, 900, 1100, 1200, 1300 and 1400. References: available in figures 1–4.

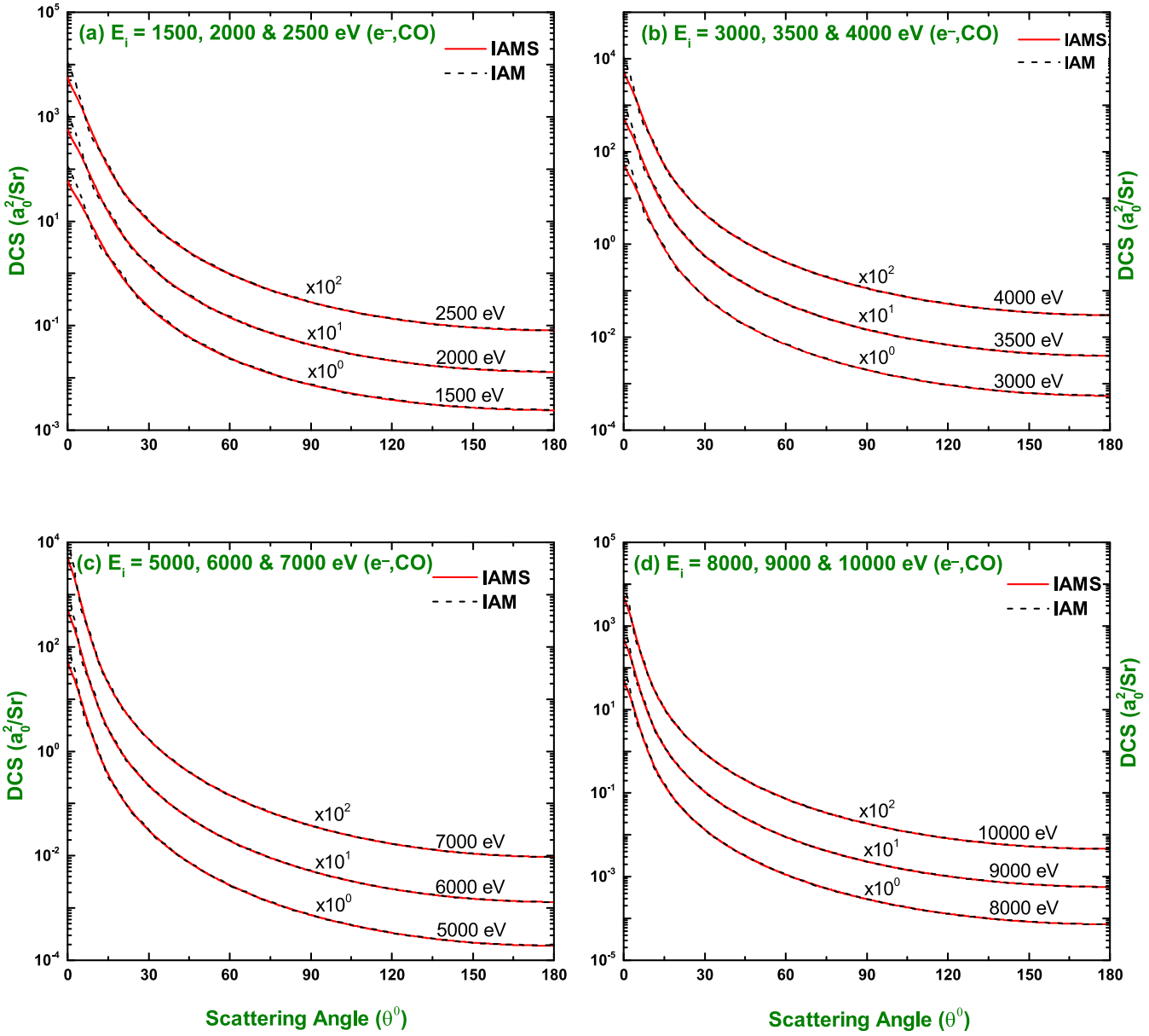

Figure 6. DCS (a_0^2/Sr) for the same as in figure 1 at energies 1500, 2000, 2500, 3000, 3500, 4000, 5000, 6000, 7000, 8000, 9000 and 10 000 eV.

and can be used as the recommended set of cross sections. This is why we have extended our DCS calculations up to 10 keV. From this figure, it is visible that the experimental cross sections at 900 and 1100 eV of [14] are same and sudden fall of cross sections at 1300 eV poses doubt about the authenticity of data at 1300 eV. Our IAMS calculations appear as the mean of the experimental data within the data range and as extrapolation beyond the range. Although these plots are revealing the consistency and reliability of our calculations, we are expecting at least one more set of data (either theoretical or experimental) at 1100 and 1300 eV, to establish a reference set of DCS data for electron scattering by CO molecule. It observed that the DCS maximum occurs at the $\theta = 0^\circ$ at all energies. This is due to the interference of incident wave and that scattered from the forward direction. The optical theorem bears testimony to this inference. DCS minima, sharp or flat occur up to around 200 eV, but disappear at higher energies. Unlike the scattering from atoms, a single minimum features the scattering from CO molecule. A minimum in DCS is formed due to destructive interference of waves scattered from bound electrons. At higher energies, the structure disappears and leads to monotonous pattern of DCS due to the short interaction time.

In figures 8(a)–(f), we depict our calculated DCS of positron scattering at energies 5.25, 6.75, 10, 20, 50 and 100 eV and compare with the measured scattering data of Przybyla *et al* [15] and Sullivan *et al* [65]. A calculation of Arretche *et al* [45] shows significant disagreement with experimental data. Below 20 eV, we see significant discrepancies in magnitude and fair concordance in pattern of our calculations with

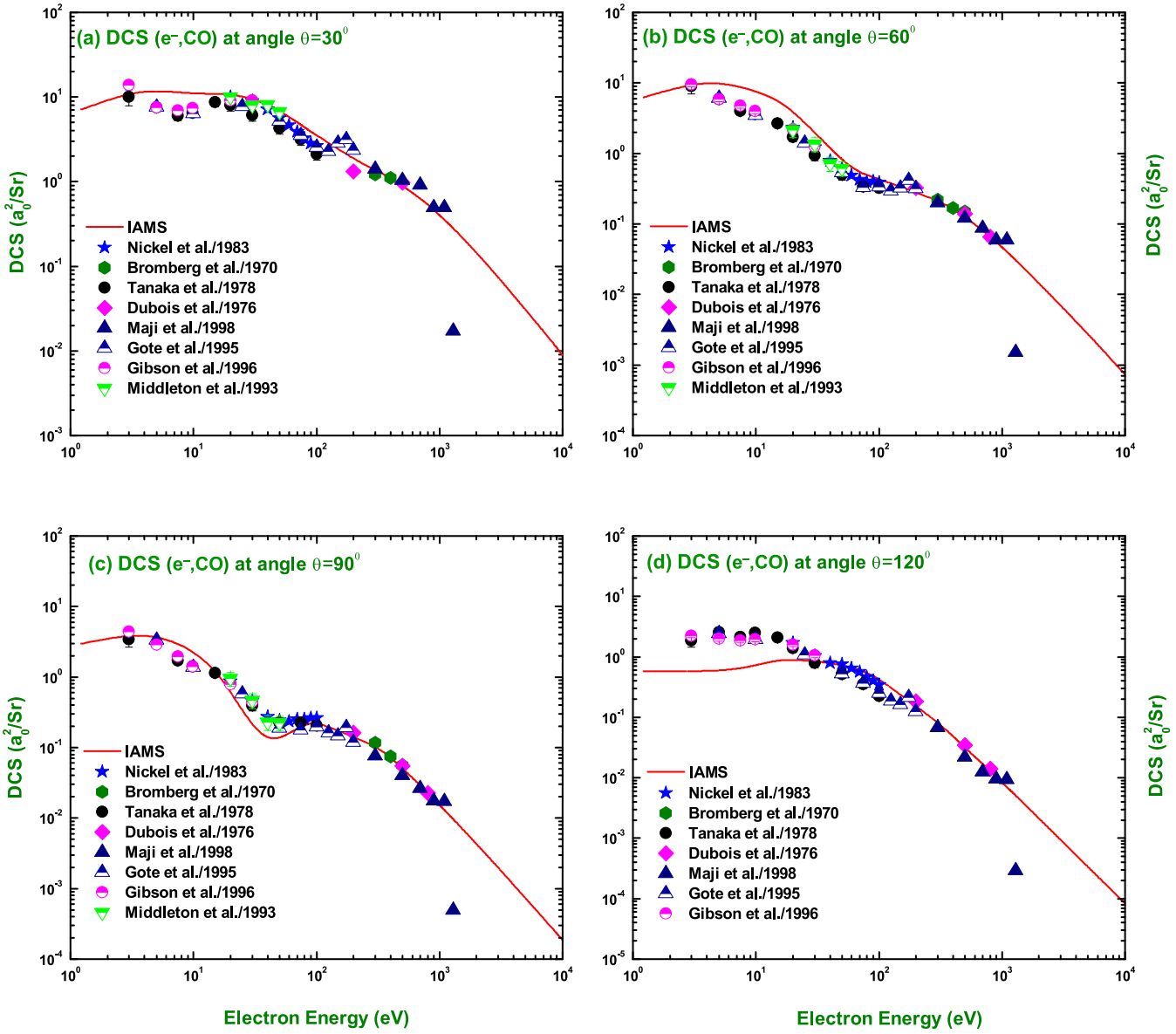

Figure 7. Energy dependence of DCS (a_0^2/Sr) for the elastic scattering of electrons from CO at angles 30°, 60°, 90° and 120°. References: available in figures 1–6.

data. However at 20 eV, the quality of fit of our results to the data improves. A very close agreement at energies 50 and 100 eV is obtained. We think, the disagreement in low energy region of our calculations with the measured values are due to the same reasons as that of electron. In addition to those, another reason might be the lack of pure elastic scattering data. These data [15] are quasi-elastic with positrons that have elastically scattered and rotational or vibrational excitations have significant contribution to elastic scattering at low energy region and lesser contribution at high energy region. In figure 9, we present our calculations over the wide energy range (150–10 000 eV). There is no DCS data (either theoretical or experimental) of e^+–CO collision in the intermediate and high energy domain. We have applied the AR to positron–atom scattering data of Dapor & Miotello [66] at energies 500, 1000, 1500, 2000, 2500, 3000, 3500 and 4000 eV to calculate e^+–CO scattering cross-sections from those of C and O atoms to compare with our IAM and IAMS calculations. We find close agreement in shape but differences in magnitude (since the approaches are different) with our calculations and the difference gradually decreases with increasing impact energy. At 4000 eV, the data of [66] almost merge with both of our approaches (IAM and IAMS), implying that at high energy region the IAM, IAMS and additive approximation reproduce the same cross sections in case of simple di-atomic molecule like CO. In the similar way, we also compare our calculated IECS, MTCS and VCS with the corresponding cross sections derived from the atomic data of [66] in figures 15(c), (e) and (f) and find close agreements in all the cases. This result indicates that the screening and structure effect are negligible, and the incident projectile sees the molecule as a single entity at these high energies.

In figures 10 and 11, we present the variation of DCSs with energy for electron and positron, respectively. The interference

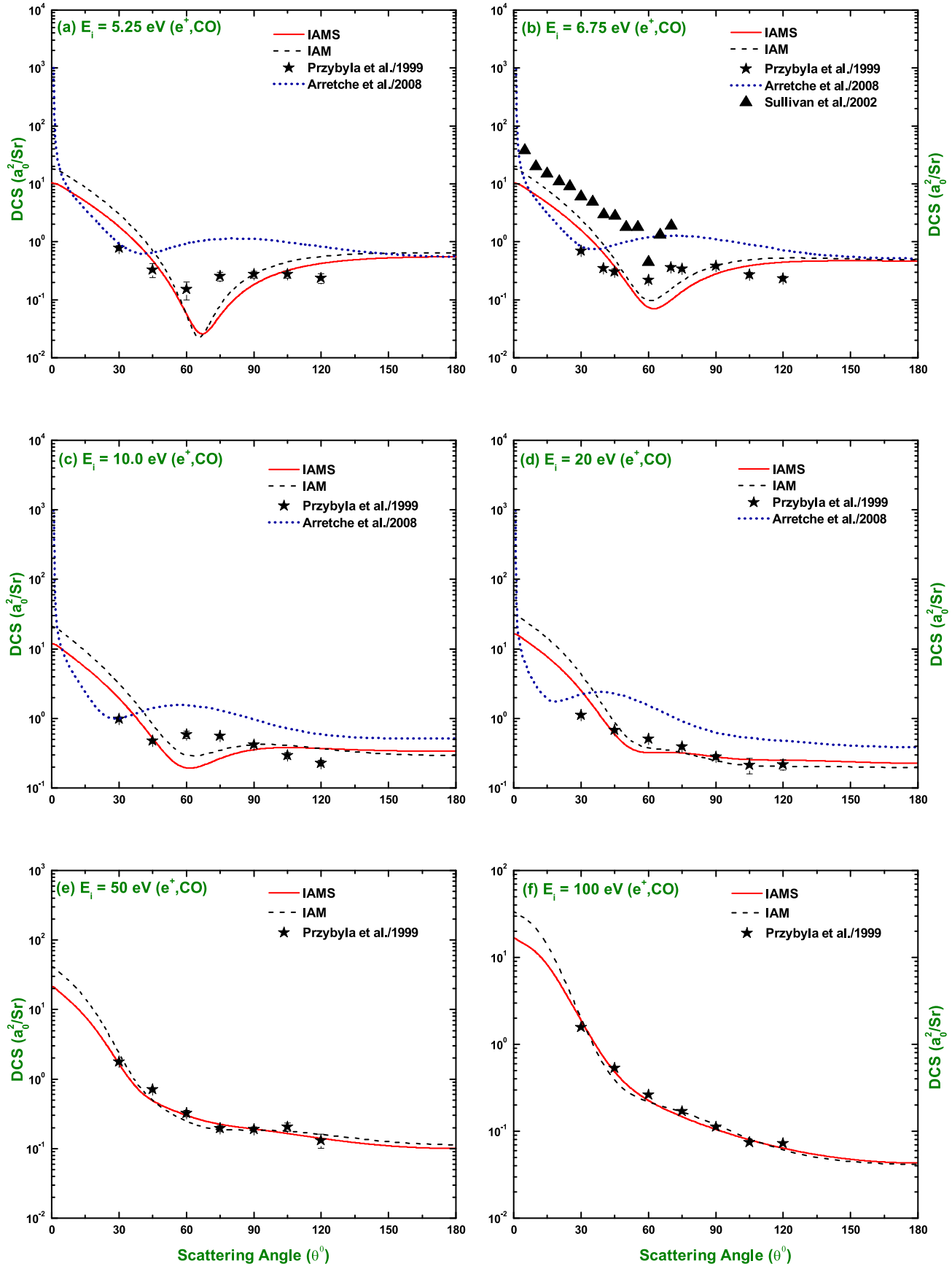

Figure 8. DCS (a_0^2/Sr) for the elastic scattering of positron from CO at energies 5.25, 6.75, 10, 20, 50 and 100 eV. Theoretical: IAM, IAMS and Arretche *et al* [45]. Experimental: Przybyla *et al* [15] and Sullivan *et al* [65].

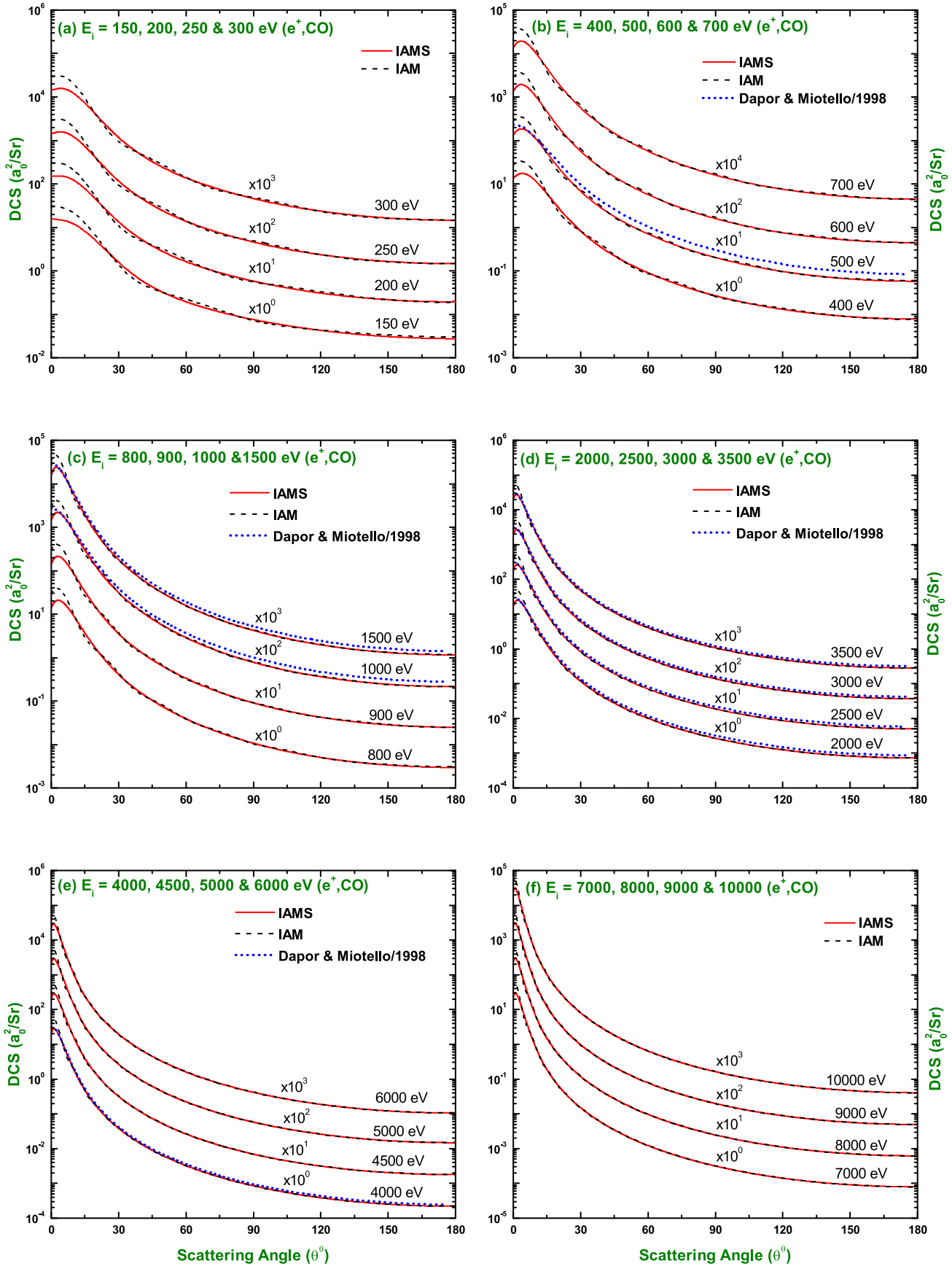

Figure 9. DCS (a_0^2/Sr) for the same as in figure 8 at energies 150, 200, 250, 300, 400, 500, 600, 700, 800, 900, 1000, 1500, 2000, 2500, 3000, 3500, 4000, 4500, 5000, 6000, 7000, 8000, 9000 and 10 000 eV. References: available in figure 8 and Dapor & Miotello [66].

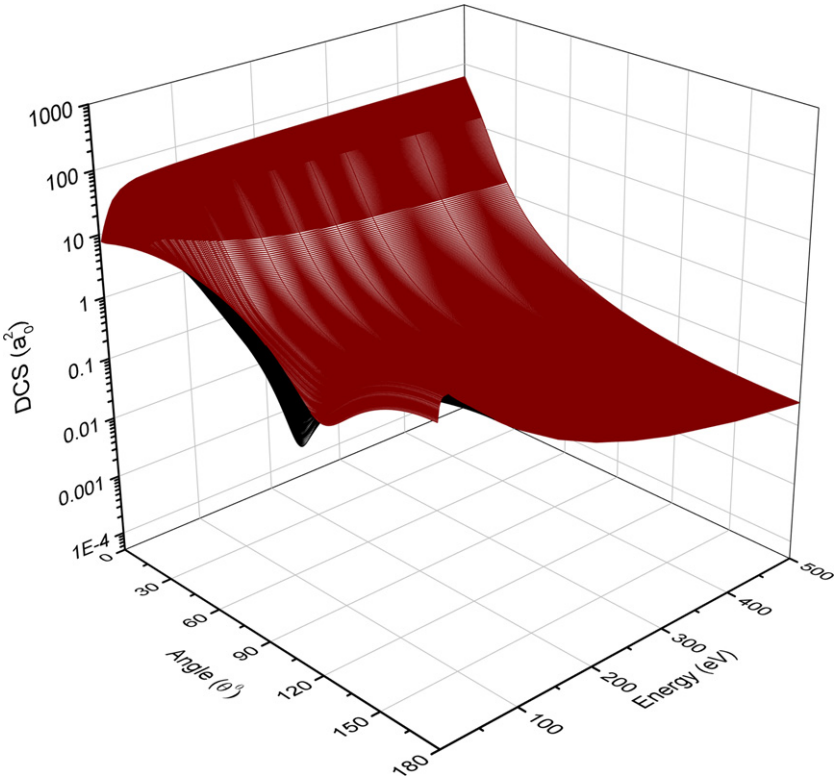

Figure 10. Variation of DCS (a_0^2/Sr) for the elastic scattering of electrons from CO.

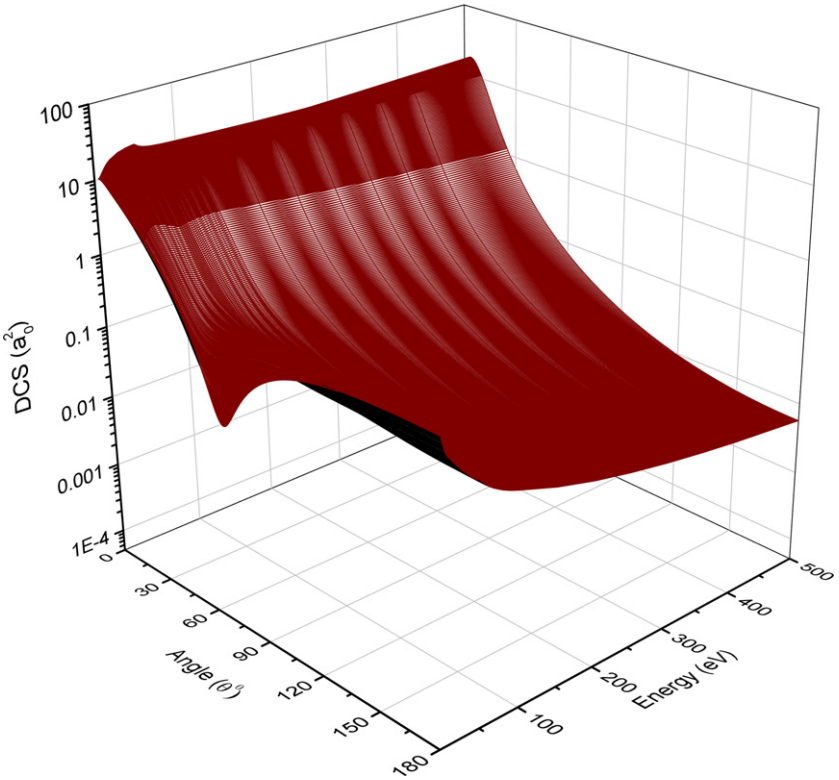

Figure 11. Variation of DCS (a_0^2/Sr) for the elastic scattering of positrons from CO.

structure disappears in DCS at higher energies because of short duration of interaction between the projectile and molecule [6]. In figures 12 and 13, Sherman function $S(\theta)$ is presented for electron and positron, respectively. For the first time, so far as our knowledge goes, we are reporting the spin-polarization of $e^{\pm}$–CO scattering. Employing AR on atomic polarization

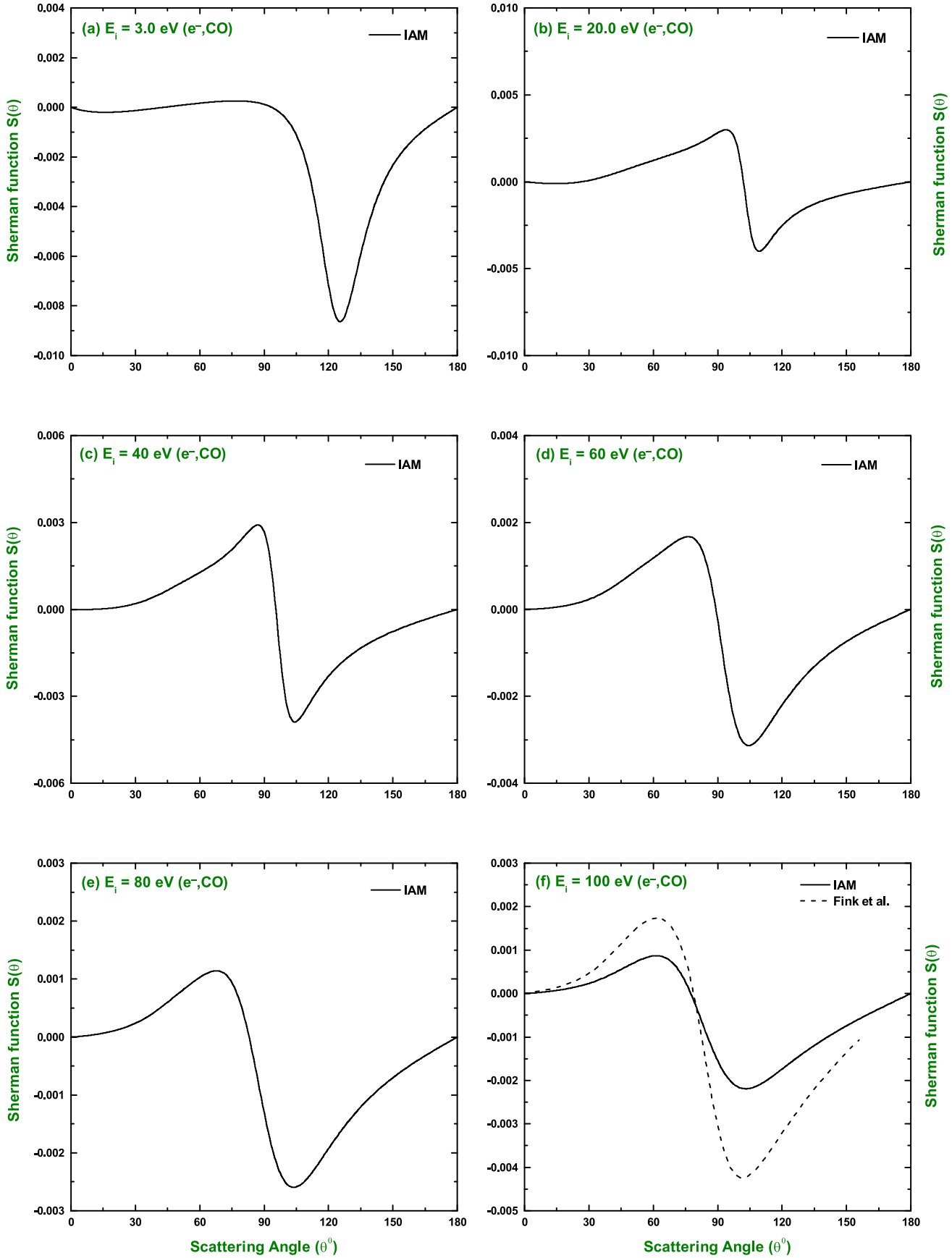

Figure 12. Angular dependence of the scattered electron spin-polarization. Theoretical: IAM, Fink and Yates [67] and Fink and Ingram [68].

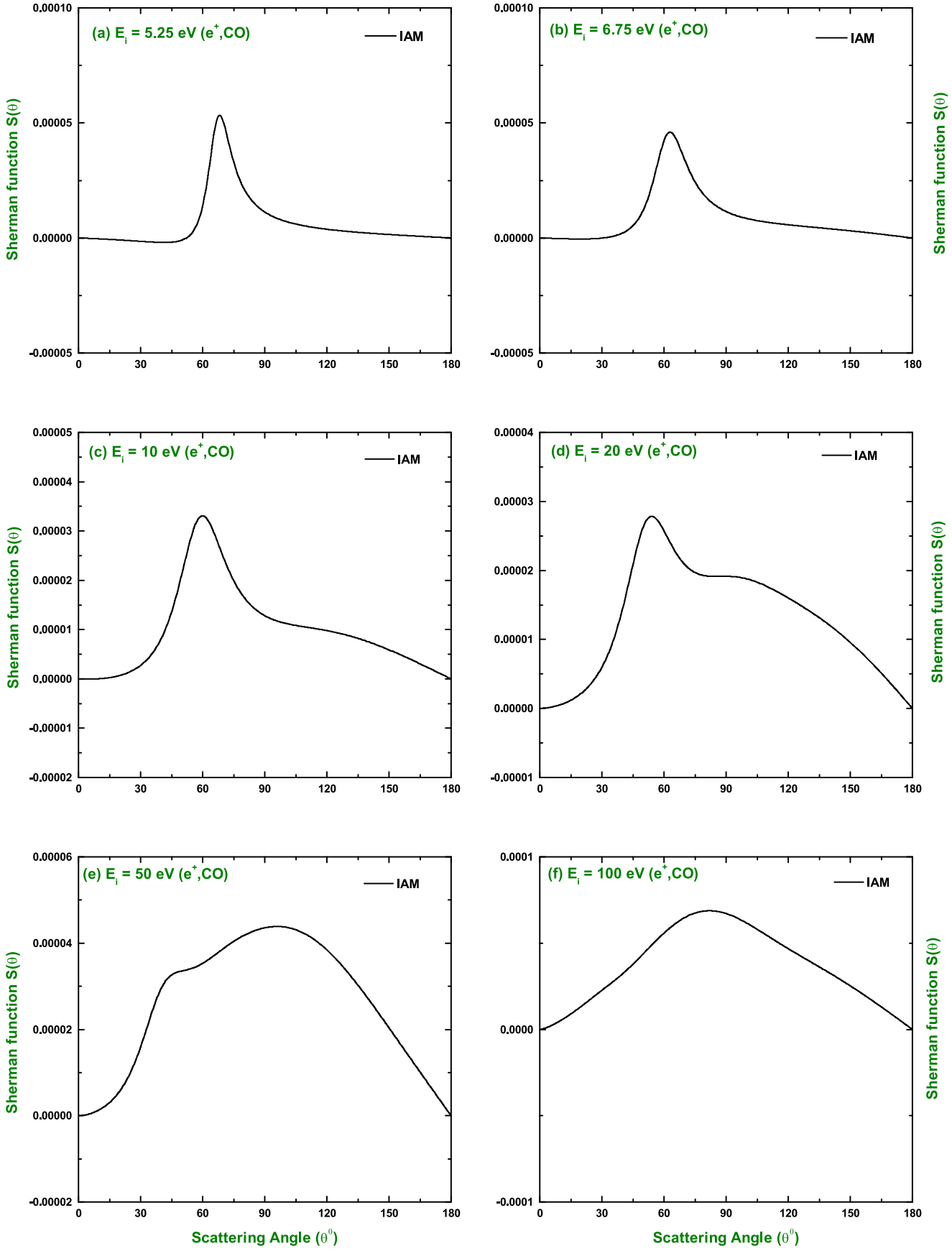

Figure 13. Angular dependence of the scattered positron spin-polarization. Theoretical: IAM.

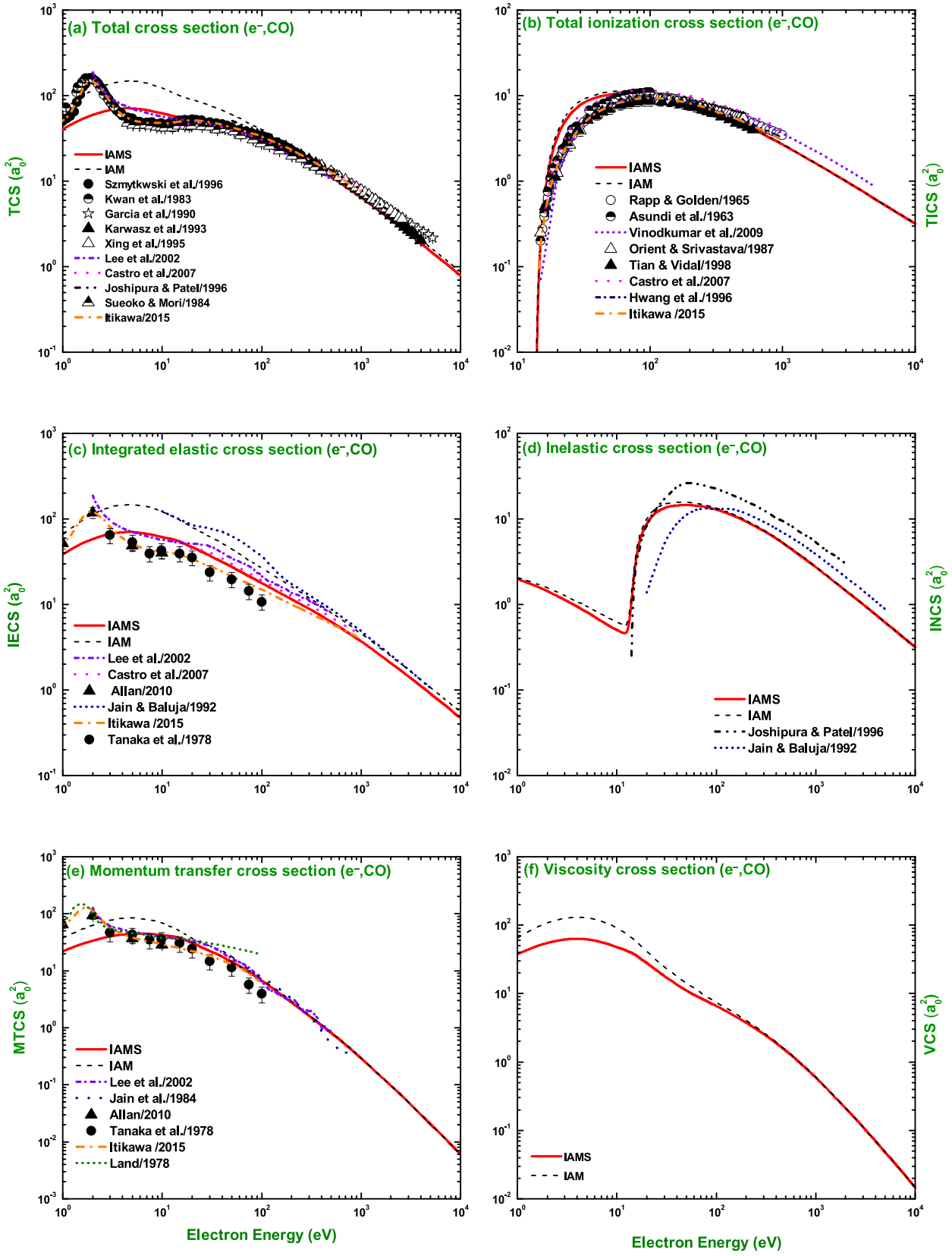

Figure 14. TCS, TICS, IECS, INCS, MTCS and VCS (a_0^2) for the scattering of electrons from CO. Theoretical: IAM, IAMS, Jain *et al* [2], Itikawa [5], Lee *et al* [34], Castro *et al* [35], Joshipura and Patel [36], Vinodkumar *et al* [38], Hwang *et al* [39], Jain and Baluja [40] and Land [41]. Experimental: Szmytkowski *et al* [1], Tanaka *et al* [4], Garcia *et al* [19], Karwasz *et al* [20], Xing *et al* [21], Kwan *et al* [22], Sueoko and Mori [23], Rapp and Golden [26], Asundi *et al* [27], Orient and Srivastava [28], Tian and Vidal [29] and Alan [30].

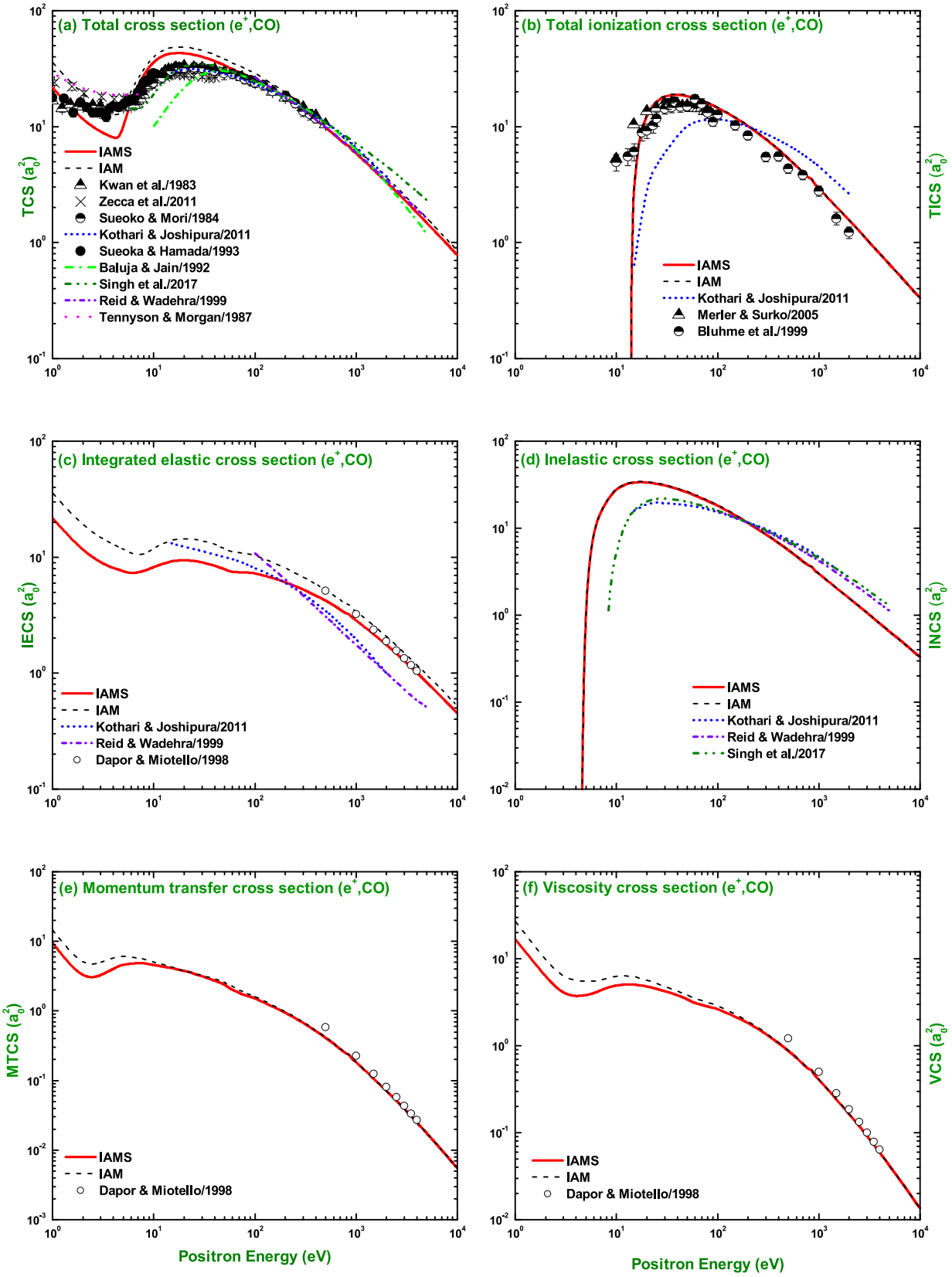

Figure 15. TCS, TICS, IECS, INCS, MTCS and VCS (a_0^2) for the scattering of positrons from CO. Theoretical: IAM, IAMS, Singh *et al* [3], Kothari and Joshipura [42], Baluja and Jain [43], Reid and Wadehra [44], Dapor and Miotello [66] and Tennyson and Morgan [69]. Experimental: Kwan *et al* [22], Sueoka and Hamada [23], Zecca *et al* [24], Sueoka and Mori [25], Marler and Surko [31] and Bluhme *et al* [32].

data of Fink and Yates [67] and Fink and Ingram [68], e^-–CO spin-polarization data at 100 eV is generated and presented in figure 12(f) to compare with our calculations. We find a fairly good agreement in pattern with differences in magnitude. This is not unexpected as $S(\theta)$ is highly sensitive, like the phase-shifts, to the variation of the procedure used to generate it.

In figure 14, we depict TCS, TICS, IECS, INCS, MTCS and VCS for the scattering of electron from CO molecule in the 1–10 000 eV energy range, in comparison with the existing experimental and theoretical results. As figure 14(a) shows, our IAMS and the calculations of [34, 35] are in a good agreement with the experimental TCS data of [1, 20–23], from 15 eV to the highest energy available in literature. Calculations of [34] are available in 2–500 eV energy range and that of [35] are in 15–1000 eV range. Our IAMS results and those of [34] agree closely from 3 eV to last point of the latter. No theoretical calculations are able to produce the 2Π shape resonance in the vicinity of 2 eV and hump at $\sim$8 eV except broader resonance around 20 eV. Theoretical formulations like *R*-matrix or multichannel calculations might be able to reproduce these special features in low energy domain. In figure 14(b), we present our theoretical calculations of TICS caused by electron, with the experimental [26–29], theoretical [38, 39] results, and also recommended data of Itikawa [5]. Our calculations agree reasonably except in the 20–45 eV energy range. In figure 14(c), we compare our theoretical calculations of IECS, with experimentally measured data [4, 30] and theoretical calculations [34, 35, 40]. Although our IAMS calculations cannot reproduce the shape resonance around 2 eV, these lie closest to the experimental data among all the theoretical calculations compared with. All the theoretical calculations overestimate the experimental measurements largely. In figure 14(d), our calculated INCS are presented along with the calculations of Joshipura and Patel [36] and Jain and Baluja [40]. Both the calculations overestimated, apart from low energies where a jumble of lower and higher values of the cross sections than ours are present. Our TICS (shown in 14 (b)) calculations are based on the INCS data showing a better agreement with experimental observations from energy 45 eV and upwards, so we are expecting that our calculated INCS, is more reliable and can be used as the recommended cross sections. In figure 14(e), we present our theoretical calculations of MTCS in comparison with the experimental measurements [4, 30] and theoretical calculations [2, 34, 41]. As seen in the figure, the calculations of Land [41] shows a good agreement with experimental data up to 15 eV but a noticeable disagreement is observed beyond that energy. Our IAMS calculations shows reasonably good agreement with the experimental data and those of Lee *et al* [34]. In figure 14(f), we present our calculated VCS.

In figures 15(a)–(f), we present TCS, TICS, IECS, INCS, MTCS and VCS for the scattering of positron from CO. We observe a reasonably good agreement between our calculations with the experimental data [22–25] and the calculated data from atomic scattering by [66]. Figure 15(a) shows differences among the experimental data of positron impact TCS in low energy region (1–7 eV). This disagreement decreases with increase of energy up to about 40 eV beyond which, all the measurements overlap. *R*-matrix calculation of Tennyson and Morgan [69] makes close agreement with [24] but overestimates the experimental data of [22, 25]. The TCS suddenly increases from $\sim$7 eV, signifying the Ps formation, a very unique feature of positron impact collisions. The Ps formation threshold for CO is 7.2 eV [15]. A broad resonance is observed in and around 20 eV. Our calculations are consistent with the experimental data except the resonance region. Although our findings overestimate the data around the peak region but follow the pattern of the experimental data. We notice a close agreement of our results at $\geqslant$50 eV. From 60 eV, all the theoretical calculations agree with one another, except those of Singh *et al* [3]. Although their calculations [3] produce a good agreement with the data from 20 to 500 eV, these results lie above all the other theoretical calculations for the energies $>$500 eV. In figure 15(b), we present our calculations for TICS along with the measured values [31, 32] and the theoretical calculation [42]. Our calculations produce a reasonably good agreement with the experimental data. Calculations of Kothari and Joshipura [42] show a profound disagreement with the experimental data and our calculations. In figures 15(c) and (d), we have compared our IAM and IAMS results of IECS and INCS with those of [42, 44]. Noticeable disagreement is observed between our calculations with those of [42, 44]. We have calculated the INCS data of [44] from their TCS and IECS data to compare with ours.

4. Conclusion

We report results of our calculations of various scattering observables for the $e^{\pm}$–CO scattering systems in a wide energy range (1–10 000 eV), in the framework of Dirac partial wave analysis. Dirac relativistic equation is solved numerically to get the values of DCS, TCS, IECS, INCS, MTCS, VCS, TICS and spin-polarization. A complex OMP is used to represent the $e^{\pm}$–CO interactions. For the first time, we are reporting the several collision cross sections over such a wide range of energies. We have compared our results with the existing experimental data and other available theoretical calculations. The calculations are carried out with the inclusion of screening correction in the single scattering IAM. This correction is included in the collision dynamics to account for the mutual overlapping of the nearby atomic orbitals of molecules. The study has demonstrated that the incorporation of the screening effect in theory reduces the cross sections at low energies and angles, thereby improving the quality of the predicted results. This study shows that the IAM and IAMS results are too close to be distinguishable at higher energies, indicating that the screening effect is negligible at such energies. This investigation of projectile–CO scattering buttresses the usefulness of this model to predict data for various scattering observables of $e^{\pm}$–molecule scattering. Our calculated results for DCS, TCS, IECS, INCS, MTCS, VCS, TICS and Sherman function using IAMS, agree closely with the available experimental data and other sophisticated calculations for both projectiles (e^- and e^+). So, the IAMS method emerges out as an effective procedure for the generation of wealth of numerical data, from 50 eV to the highest energy considered herein.

The inclusion of exchange, polarization potentials and screening correction in the collision dynamics improves the

outputs of the present IAMS method at low energies and angles. However, this is not a panacea. Sophisticated methods using realistic projectile–molecule interaction perform well at low energies undoubtedly at the expense of lengthy, cumbersome, time-consuming and some approximations. The present rather easy-to-implement method generates reasonably accurate molecular data useful for modeling in science and technologies. The success of the present IAMS procedure with the inclusion of the screening effect in describing the scattering of electron and positron with reasonable accuracy is encouraging and holds a promise. This handy procedure might be used to generate useful data for other di-atomic and polyatomic molecules having importance in modeling material and biological processes. More data is needed for further refinement of the theory.

Acknowledgments

M Masum Billah and Mahmudul H Khandker thankfully acknowledge University of Rajshahi for the partial funding through the project no-5/52/RU/Science-2/18–19.

Data availability statement

All data that support the findings of this study are included within the article (and any supplementary files).

ORCID iDs

M Masum Billah https://orcid.org/0000-0001-6987-0977
Mahmudul H Khandker https://orcid.org/0000-0001-9097-923X
M Shorifuddoza https://orcid.org/0000-0003-1904-4604
M A Sayed https://orcid.org/0000-0002-1288-2800
Hiroshi Watabe https://orcid.org/0000-0001-6257-7735
A K F Haque https://orcid.org/0000-0002-1735-3967
M Alfaz Uddin https://orcid.org/0000-0003-3911-0074

References

[1] Szmytkowski C, Maciag K and Karwasz G 1996 Absolute electron-scattering total cross section measurements for noble gas atoms and diatomic molecules *Phys. Scr.* **54** 271
[2] Jain A, Freitas L C G, Mu-Tao L and Tayal S S 1984 Elastic scattering of intermediate and high energy electrons with N_2 and CO molecules *J. Phys. B: At. Mol. Phys.* **17** L29
[3] Singh S, Dutta S, Naghma R and Antony B 2017 Positron scattering from simple molecules *J. Phys. B: At. Mol. Opt. Phys.* **50** 135202
[4] Tanaka H, Srivastava S K and Chutjian A 1978 Absolute elastic differential electron scattering cross sections in the intermediate energy region. IV. Co *J. Chem. Phys.* **69** 5329–33
[5] Itikawa Y 2015 Cross sections for electron collisions with carbon monoxide *J. Phys. Chem. Ref. Data* **44** 013105
[6] Khandker M H, Arony N T, Haque A K F, Maaza M, Billah M M and Uddin M A 2019 Scattering of $e^{\pm}$ from N_2 in the energy range 1 eV–10 keV *Mol. Phys.* 1–15
[7] Salvat F, Jablonski A and Powell C J 2005 Elsepa–Dirac partial-wave calculation of elastic scattering of electrons and positrons by atoms, positive ions and molecules *Comput. Phys. Commun.* **165** 157–90
[8] Blanco F, Ellis-Gibbings L and García G 2016 Screening corrections for the interference contributions to the electron and positron scattering cross sections from polyatomic molecules *Chem. Phys. Lett.* **645** 71–5
[9] Blanco F and Garcia G 2003 Screening corrections for calculation of electron scattering from polyatomic molecules *Phys. Lett.* A **317** 458–62
[10] Gholami N, Hajivaliei M and Samei M E 2019 Calculation of electron scattering cross sections for anthracene, pyridine and warfarin molecules over energy range 10–30000 eV *Appl. Radiat. Isot.* **150** 79–86
[11] Gibson J C, Morgan L A, Gulley R J, Brunger M J, Bundschu C T and Buckman S J 1996 Low energy electron scattering from CO: absolute cross section measurements and *R*-matrix calculations *J. Phys. B: At. Mol. Opt. Phys.* **29** 3197
[12] Gote M and Ehrhardt H 1995 Rotational excitation of diatomic molecules at intermediate energies: absolute differential state-to-state transition cross sections for electron scattering from N_2, Cl_2, CO and HCl *J. Phys. B: At. Mol. Opt. Phys.* **28** 3957
[13] Middleton A G, Brunger M J and Teubner P J O 1993 Excitation of the electronic states of carbon monoxide by electron impact *J. Phys. B: At. Mol. Opt. Phys.* **26** 1743
[14] Maji S, Basavaraju G, Bharathi S M, Bhushan K G and Khare S P 1998 Elastic scattering of electrons by polyatomic molecules in the energy range 300–1300 eV: CO, CO_2, CH_4, C_2H_4 and C_2H_6 *J. Phys. B: At. Mol. Opt. Phys.* **31** 4975
[15] Przybyla D A, Addo-Asah W, Kauppila W E, Kwan C K and Stein T S 1999 Measurements of differential cross sections for positrons scattered from N_2, CO, O_2, N_2O, and CO_2 *Phys. Rev.* A **60** 359
[16] Nickel J C, Mott C, Kanik I and McCollum D C 1988 Absolute elastic differential electron scattering cross sections for carbon monoxide and molecular nitrogen in the intermediate energy region *J. Phys. B: At. Mol. Opt. Phys.* **21** 1867
[17] DuBois R D and Rudd M E 1976 Differential cross sections for elastic scattering of electrons from argon, neon, nitrogen and carbon monoxide *J. Phys. B: At. Mol. Phys.* **9** 2657
[18] Bromberg J P 1970 Absolute differential cross sections of elastically scattered electrons. III CO and N_2 at 500, 400, and 300 eV *J. Chem. Phys.* **52** 1243–7
[19] Garca G, Aragón C and Campos J 1990 Total cross sections for electron scattering from CO in the energy range 380–5200 eV *Phys. Rev.* A **42** 4400
[20] Karwasz G, Brusa R S, Gasparoli A and Zecca A 1993 Total cross-section measurements for e^--CO scattering: 80–4000 eV *Chem. Phys. Lett.* **211** 529–33
[21] Xing S L, Shi Q C, Chen X J, Xu K Z, Yang B X, Wu S L and Feng R F 1995 Absolute total-cross-section measurements for intermediate-energy electron scattering on C_2H_2 and CO *Phys. Rev.* A **51** 414
[22] Kwan C K, Hsieh Y F, Kauppila W E, Smith S J, Stein T S, Uddin M N and Dababneh M S 1983 $e^{\pm}$–CO and $e^{\pm}$–CO_2 total cross-section measurements *Phys. Rev.* A **27** 1328
[23] Sueoka O and Mori S 1984 Total cross-sections for positrons and electrons colliding with N_2, CO and CO_2 molecules *J. Phys. Soc. Japan* **53** 2491–500
[24] Zecca A, Chiari L, Sarkar A and Brunger M J 2011 Positron scattering from the isoelectronic molecules N_2, CO and C_2H_2 *New J. Phys.* **13** 115001
[25] Sueoka O and Hamada A 1993 Total cross-section measurements for 0.3–10 eV positron scattering on N_2, CO, and CO_2 molecules *J. Phys. Soc. Japan* **62** 2669–74
[26] Rapp D and Englander-Golden P 1965 Total cross sections for ionization and attachment in gases by electron impact. I. Positive ionization *J. Chem. Phys.* **43** 1464–79
[27] Asundi R K, Craggs J D and Kurepa M V 1963 Electron attachment and ionization in oxygen, carbon monoxide and carbon dioxide *Proc. Phys. Soc.* **82** 967

[28] Orient O J and Strivastava S K 1987 Electron impact ionisation of H_2O, CO, CO_2 and CH_4 *J. Phys. B: At. Mol. Phys.* **20** 3923

[29] Tian C and Vidal C R 1998 Cross sections of the electron impact dissociative ionization of CO *J. Phys. B: At. Mol. Opt. Phys.* **31** 895

[30] Allan M 2010 Electron collisions with CO: elastic and vibrational excitation cross sections *Phys. Rev.* A **81** 042706

[31] Marler J P and Surko C M 2005 Positron-impact ionization, positronium formation, and electronic excitation cross sections for diatomic molecules *Phys. Rev.* A **72** 062713

[32] Bluhme H, Frandsen N P, Jacobsen F M, Knudsen H, Merrison J, Paludan K and Poulsen M R 1998 Non-dissociative and dissociative ionization of nitrogen molecules by positron impact *J. Phys. B: At. Mol. Opt. Phys.* **31** 4631

[33] Jain A 1982 Elastic scattering of intermediate- and high-energy electrons by N_2 and CO in the two-potential coherent approach *J. Phys. B: At. Mol. Phys.* **15** 1533

[34] Lee M-T, Iga I, Brescansin L M, Machado L E and Machado F B C 2002 Theoretical studies on electron–carbon monoxide collisions in the low and intermediate energy range *J. Mol. Struct.: THEOCHEM* **585** 181–7

[35] Castro E A y, Souza G L C d, Iga I, Machado L E, Brescansin L M and Lee M-T 2007 Absorption effects for electron–molecule collisions *J. Electron Spectrosc. Relat. Phenom.* **159** 30–8

[36] Joshipura K N and Patel P M 1996 Total electron scattering cross sections for NO, CO, NO_2, N_2O, CO_2 and NH_3 ($E_i \geq 50$ eV) *J. Phys. B: At. Mol. Opt. Phys.* **29** 3925

[37] Kanik I, Trajmar S and Nickel J C 1993 Total electron scattering and electronic state excitations cross sections for O_2, CO, and CH_4 *J. Geophys. Res.* **98** 7447–60

[38] Vinodkumar M, Limbachiya C and Bhutadia H 2009 Electron impact calculations of total ionization cross sections for environmentally sensitive diatomic and triatomic molecules from threshold to 5 keV *J. Phys. B: At. Mol. Opt. Phys.* **43** 015203

[39] Hwang W, Kim Y K and Rudd M E 1996 New model for electron-impact ionization cross sections of molecules *J. Chem. Phys.* **104** 2956–66

[40] Jain A and Baluja K L 1992 Total (elastic plus inelastic) cross sections for electron scattering from diatomic and polyatomic molecules at 10–5000 eV: H_2, Li_2, HF, CH_4, N_2, CO, C_2H_2, HCN, O_2, HCl, H_2S, PH_3, SiH_4, and CO_2 *Phys. Rev.* A **45** 202

[41] Land J E 1978 Electron scattering cross sections for momentum transfer and inelastic excitation in carbon monoxide *J. Appl. Phys.* **49** 5716–21

[42] Kothari H N and Joshipura K N 2011 Total and ionization cross-sections of N_2 and CO by positron impact: theoretical investigations *Pramana J. Phys.* **76** 477–88

[43] Baluja K L and Jain A 1992 Total (elastic and inelastic) scattering cross sections for several positron-molecule systems at 10–5000 eV: H_2, H_2O, NH_3, CH_4, N_2, CO, C_2H_2, O_2, SiH_4, CO_2, N_2O, and CF_4 *Phys. Rev.* A **45** 7838

[44] Reid D D and Wadehra J M 1999 Scattering of intermediate-energy positrons by C, N, O atoms and the corresponding diatomic molecules: elastic and total cross-sections *Chem. Phys. Lett.* **311** 385–9

[45] Arretche F, Mazon K T, Michelin S E, Fujimoto M M, Iga I and Lee M-T 2008 Low energy elastic scattering of positrons by CO: an application of continued fractions and schwinger variational iterative methods *Nucl. Instrum. Methods Phys. Res.* B **266** 441–6

[46] Dora A and Tennyson J 2020 Electron collisions with CO molecule: potential energy curves of higher lying CO^- resonant states *J. Phys. B: At. Mol. Opt. Phys.* **53** 195202

[47] Dora A, Tennyson J and Chakrabarti K 2016 Higher lying resonances in low-energy electron scattering with carbon monoxide *Eur. Phys. J.* D **70** 1–10

[48] Sun Q, Winstead C and McKoy V 1992 Electronic excitation of carbon monoxide by low-energy electron impact *Phys. Rev.* A **46** 6987

[49] Zawadzki M, Khakoo M A, Logan V, Ratkovich L, Mašín Z, Houfek K, Dora A, Laher R and Tennyson J 2020 Low energy inelastic electron scattering from carbon monoxide: I. excitation of the $a3\pi$, $a3\sigma^+$ and $a1\pi$ electronic states *J. Phys. B: At. Mol. Opt. Phys.* **53** 165201

[50] da Silva E P, Varella M T d N and Lima M A P 2005 Electronic excitation of CO by positron impact *Phys. Rev.* A **72** 062715

[51] Hahn B, Ravenhall D G and Hofstadter R 1956 High-energy electron scattering and the charge distributions of selected nuclei *Phys. Rev.* **101** 1131

[52] Desclaux J P 1975 A multiconfiguration relativistic Dirac–Fock program *Comput. Phys. Commun.* **9** 31–45

[53] Furness J B and McCarthy I E 1973 Semiphenomenological optical model for electron scattering on atoms *J. Phys. B: At. Mol. Phys.* **6** 2280

[54] Salvat F 2003 Optical-model potential for electron and positron elastic scattering by atoms *Phys. Rev.* A **68** 012708

[55] Perdew J P and Zunger A 1981 Self-interaction correction to density-functional approximations for many-electron systems *Phys. Rev.* B **23** 5048

[56] Jain A 1990 Low-energy positron-argon collisions by using parameter-free positron correlation polarization potentials *Phys. Rev.* A **41** 2437

[57] Walker D W 1971 Relativistic effects in low energy electron scattering from atoms *Adv. Phys.* **20** 257–323

[58] Francis Mott N *et al* 1965 *The Theory of Atomic Collisions* vol 35 (Oxford: Clarendon)

[59] Khandker M H, Billah M M, Watabe H, Haque A K F and Uddin M A 2020 Theoretical studies on the elastic scattering of $e^{\pm}$ off the ions of xenon isonuclear series *Phys. Scr.* **96** 025402

[60] Lide D R 2004 *CRC Handbook of Chemistry and Physics* vol 85 (Boca Raton, FL: CRC Press)

[61] Zhan C-G, Nichols J A and Dixon D A 2003 Ionization potential, electron affinity, electronegativity, hardness, and electron excitation energy: molecular properties from density functional theory orbital energies *J. Phys. Chem.* A **107** 4184–95

[62] Joshipura K N and Antony B K 2001 Total (including ionization) cross sections of electron impact on ground state and metastable Ne atoms *Phys. Lett.* A **289** 323–8

[63] Joshipura K N and Limbachiya C G 2002 Theoretical total ionization cross-sections for electron impact on atomic and molecular halogens *Int. J. Mass Spectrom.* **216** 239–47

[64] Joshipura K N, Vinodkumar M, Limbachiya C G and Antony B K 2004 Calculated total cross sections of electron-impact ionization and excitations in tetrahedral (XY_4) and SF_6 molecules *Phys. Rev.* A **69** 022705

[65] Sullivan J P, Gilbert S J, Marler J P, Barnes L D, Buckman S J and Surko C M 2002 Low energy positron scattering and annihilation studies using a high resolution trap-based beam *Nucl. Instrum. Methods Phys. Res.* B **192** 3–16

[66] Dapor M and Miotello A 1998 Differential, total, and transport cross sections for elastic scattering of low energy positrons by neutral atoms ($Z = 1$–92, $E = 500$–4000 eV) *At. Data Nucl. Data Tables* **69** 1–100

[67] Fink M and Yates A C 1969 Theoretical electron scattering amplitudes and spin polarizations *At. Data Nucl. Data Tables* **1** 385–456

[68] Fink M and Ingram J 1972 Theoretical electron scattering amplitudes and spin polarizations *At. Data Nucl. Data Tables* **4** 129–207

[69] Tennyson J and Morgan L 1987 Rotational and polarisation effects in low-energy positron-CO collisions using the *R*-matrix method *J. Phys. B: At. Mol. Phys.* **20** L641